Journal of Rehabilitation in Civil Engineering 13-4 (2025) 81-109

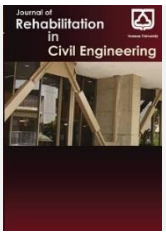

Journal of Rehabilitation in Civil Engineering

Journal homepage: https://civiljournal.semnan.ac.ir/

Seismic Evaluation of Steel Plate Shear Walls in Different Configurations

Seyed Mohammad Ali Abbaspoor Haghighat [1]; Ali Alibazi [2,*]; Reza Moradifard [2]; Lotfi Guizani [3]; Munzer Hassan [3]

1. Master Graduated, Faculty of Engineering, Yasouj University, Yasouj, Iran
2. Master Graduated, Faculty of Civil, Water and Environmental Engineering, Shahid Beheshti University, Tehran, Iran
3. Department of Construction Engineering, École de technologie supérieure, University of Quebec, Quebec, Canada
* Corresponding author: *a_alibazi@yahoo.com*

ARTICLE INFO

Article history:
Received: 05 December 2024
Revised: 30 December 2024
Accepted: 14 January 2025

Keywords:
Coupled SPSW;
Coupling beam;
Performance-based plastic design;
Time-history analysis;
Incremental dynamic analysis;
IDA.

ABSTRACT

Steel plate shear walls (SPSWs) are a cost-efficient system to resist seismic lateral loads. Post-buckling strength, tension field action, and high energy absorption capacity are among the advantages of SPSWs. A beam-coupled SPSW consists of two pairs of plates connected by the coupling beam. The steel plate of a beam-coupled SPSW is typically connected to horizontal and vertical boundary elements. The connection of the steel plate to the vertical boundary elements induces an axial load and a bending moment in the plate. This research addresses the lack of comprehensive evaluations of coupled SPSWs with varying coupling beam mechanisms, such as flexural-shear behavior. Nine numerical models with different configurations and coupling degrees are developed through plastic design. Numerical analyses are carried out in SAP2000, ABAQUS, and OpenSees. Pushover, cyclic, and nonlinear time-history analyses indicate that SHEAR is the optimal model. Nonlinear static and nonlinear time-history analyses are sometimes ineffective for seismic evaluation, and incremental dynamic analysis (IDA) using FEMA P-695 demonstrate that the FLEX model can be more optimal when the construction cost and ultimate performance limit (i.e., collapse prevention (CP) limit) are incorporated. However, INT would be the most optimal model at the life safety (LS) limit.Therefore, The study provides a robust framework for optimizing seismic performance across different building heights, contributing to safer and more economical structural designs.

E-ISSN: 2345-4423

How to cite this article:
Abbaspoor Haghighat, S.M.A., Alibazi, A., Moradifard, R., Guizani, L. and Hassan, M. (2025). Seismic Evaluation of Steel Plate Shear Walls in Different Configurations. Journal of Rehabilitation in Civil Engineering, 13(4), 81-109. https://doi.org/10.22075/jrce.2025.36154.2225

1. Introduction

Steel plate shear walls (SPSWs) are a lateral load-resisting system. They are cost-efficient in high seismic hazard regions such as Japan and North America due to their ductility, post-buckling strength, and high energy absorption capacity [1,2]. SPSW strength mainly arises from the post-buckling strength of thin plates, or in other words, the diagonal tension field that forms after the buckling of the steel plate. The web steel plate is under pure shear before buckling. An increase in the load such that the compressive stress of the web would exceed the critical stress of the steel plate leads to the buckling of the plate and a wrinkled web plate. When the steel plate is used in place of diagonal members, shear in the plate induces equal tensile and compressive stresses on the side with a 45-degree inclination from the horizon. Wagner et al. performed various tests on aluminum shear panels and proposed diagonal tension field theory, demonstrating that a thin-walled panel would not become destabilized upon transverse buckling and would only diagonally deform [3]. Takahashi et al. conducted more comprehensive research on the behavior of SPSW panels and indicated that hardened SPSWs outperformed unhardened SPSWs and had a larger energy absorption capacity under cyclic loads [4]. Thorburn et al. formulated the elastic strain energy and developed an equation to estimate the tensile field angle α in an infill plate. The angle α is the angle between the vertical direction and strip direction and is measured for simple and fixed beam-column connections using Eqs. (13) and (14), respectively. These equations assume that the web plate has no compressive strength, and the tension field is a constant stress at a constant inclination angle [1]. Timler and Kulak modified the equations [5]. Tromposch and Kulak demonstrated that the strip model of Thorburn et al. yields a conservative estimate of the initial stiffness and ultimate capacity of an SPSW. They also found that the eccentricity of the connection plate had no significant effect on the behavior of SPSWs [6].

While significant progress has been made in understanding the seismic behavior of SPSWs, research on coupled SPSWs remains relatively limited. Previous studies, such as Borello and Fahnestock [7–9]. explored coupling beam mechanisms but focused primarily on single-story models or simplified configurations. Gholhaki and Ghadaksaz numerically simulated three-, eleven-, and fifteen-story frames with coupled SPSWs of rigid connections for three coupling beam lengths through the finite element method (FEM). The studied coupling beam performance using nonlinear dynamic analysis. The results showed that a reduction in the coupling beam length increased the base shear and reduced the structural period [10]. Pavir and Shekastehband and Ma et al. examined the effects of coupling beam sizes and composite wall systems, respectively, but did not provide systematic evaluations across building heights [11,12]. Also Examining the effects of inter-connection' rigidity characteristics on lateral system performance through nonlinear analyses on 4, 8, and 12-story models showed that reducing inter-connection' rigidity stiffness will lead to a decrease in the lateral capacity of the system [13].

To evaluate the effects of the beam-column connection type in the presence of concrete-filled steel columns, three models (which differed only in the beam-column connection) had the same stiffness and strength deterioration. The reduced beams and connection plates improved the performance of weld connections and delayed the failure of the connections. Furthermore, the concrete-filled steel columns improved the overall seismic performance of the system [14]. Mu and Yang (2020) experimentally and numerically analyzed the seismic behavior of two obliquely stiffened opening shear wall configurations. They demonstrated that oblique stiffeners increased the flexural capacity, torsional capacity, buckling capacity, bearing capacity, and elastic stiffness of the system. In

addition, such stiffeners lead to almost the same behavior as eccentrically braced frames, and the beam in the opening zone would function as a link beam in eccentrically braced frames. However, it should be noted that obliquely stiffened shear walls would increase the stresses of the beams [15]. Low-yield strength (LYS) steel shear plates and various beam-column connections in SPSWs were numerically and experimentally studied. The results showed that SPSWs with LYS steel shear plates had optimal stiffness, ductility, and energy dissipation under cyclic loads, and the connection type (pinned and fixed) would affect the ductility, strength, and energy absorption of the system. However, the connection type (i.e., pinned or fixed) had an insignificant effect on the stiffness of the system [16]. Analytical coupled shear wall models with the pinned outrigger system for high-rise buildings were investigated. It was found that the position of the outrigger system would be much more important than its stiffness since it is essentially a rigid member. The middle of the building height was recommended as the optimal outrigger system position, and a rise in the story-building height ratio above 0.2 would raise the effectiveness and efficiency of the outrigger system [17]. Safari-Gorji and Cheng investigated the performance-based design for coupled shear walls and conducted its plastic analysis. Their approach was efficient and minimized iterations to achieve the optimal design, meeting code provisions at different hazard levels for different interstory drifts and coupled beam rotations [18]. Pavir and Shekastehband evaluated the hysteretic behavior of the coupling beam in a coupled SPSW and demonstrated that an increase in the coupling beam section increased the shear strength and coupling degree of the beam. Furthermore, an increase in the coupling beam length raised the shear strength of the beam and reduced its coupling degree. In contrast to coupling beams, which have an insignificant contribution to shear-resisting, SPSWs and frame beams and columns have high energy absorption and shear-resisting contributions [11]. Abdollahzadeh and Malekzadeh extensively examined the ductility reduction factor, overstrength factor, and response modification factor of coupled SPSWs. They found that a reduction in the number of stories and/or an increase in the ratio of the frame height to the distance between the two two-side beam-coupled shear walls would decrease the response modification factor and ductility reduction factor. They also argued that a rise in the coupling beam depth was not an effective strategy to increase the ductility reduction factor [19]. Wu et al. experimentally investigated coupled and uncoupled weak axis-connected SPSWs and found that the weak axis prevented an abrupt and sharp column deformation. Although the coupled SPSW had higher ductility and strength, both SPSWs the maximum lateral load was resisted by the SPSW plate. Moreover, slotted steel plates raised the ductility and bearing capacity of the system and decreased the bending effect on the plate-connected beam, avoiding failure and breakage along the edge [20]. Slotted coupled SPSWs (vertical slots) were introduced as an efficient system, and their ultimate strength was formulated along with coupling degree analysis. The coupling mechanism was found to maintain ductility when the ultimate strength and energy absorption increased. Moreover, axial load reduction must be considered for inner columns connected to the coupled beam to have more cost-efficient designs [21]. SPSWs are not cost-efficient in high-rise buildings due to architectural limitations and construction costs. The beam-coupled SPSW system is an enhanced SPSW system. Beam-coupled SPSWs reduce the steel plate thickness and raise the cost-efficiency of the design. It is necessary to conduct detailed seismic evaluations of coupled SPSWs.

Steel plate shear walls (SPSWs) are a well-established lateral load-resisting system with proven seismic performance due to their ductility and energy absorption capacity. However, the optimal integration of coupling beams in SPSWs remains underexplored, especially regarding their influence on seismic behavior across different building heights. This study builds upon previous research by introducing and comparing three coupling beam configurations (flexural, flexural-shear,

and shear) within coupled SPSWs. Unlike prior studies, which predominantly focus on uncoupled SPSWs or simplified beam designs, this work evaluates coupled SPSWs through nonlinear time-history, pushover, and incremental dynamic analysis (IDA) methods. Furthermore, by utilizing FEMA P-695 guidelines, we quantify collapse capacities and propose coupling configurations tailored to low-, mid-, and high-rise structures. These contributions aim to bridge gaps in the literature by advancing both theoretical understanding and practical design strategies for coupled SPSWs.

2. Coupled SPSW design

2.1. Performance-based plastic design

This study adopted the performance-based plastic design (PBPD) approach. The PBPD estimates the distribution of the design lateral forces based on the performance obtained from time-history analysis and distributes them along the height of the structure (Eqs. (1-7)) [18,22]. Table 1 provides the PBPD parameters.

Table 1. PBPD parameters.

Parameter	Description
β_i	Shear distribution factor in story *i*
V_i & V_n	Shear forces in stories *i* and *n* (top story), respectively
W_i & W_j	Seismic weights in stories *i* and *j*, respectively
h_i & h_j	Height in stories *i* and *j*
w_n	Seismic weight in the top story
h_n	Height in the top story
T	Fundamental period of the structure
F_i & F_n	Lateral forces in stories *i* and *n*, respectively
V	Design base shear
W	Seismic weight of the structure
λ	Dimensionless parameter dependent on the period, modal characteristics, and target interstory drift
S_a	Pseudo-spectral acceleration coefficient
γ	Modification factor
C_2	A coefficient to reflect the slenderness effect in SPSW cyclic behavior
α 1	Tension field formation angle
n	Number of stories
Ve	Elastic Base Shear
Vu	Ultimate Base shear
Vy	Yield Base shear
Vh	First Hinges Base shear
Δy	Yield Drift
Δe	Elastic Drift
Δu	Ultimate Drift
μ	(Δu / Δy) Ductility Ratio
Rμ	(Ve / Vy) Reduction factor due to ductility
Rs	(Vy / Vh) Reduction factor due to overstrength
R	(Rμ * Rs = Ve / Vh) Total reduction factor
γE	(Ee + Ep: Total energy) Ee: elastic energy, Ep: plastic energy)
E	1/2 * M * S^2v: Energy formula (M: mass, Sv: spectral velocity)

Based on Kharmale and Ghosh, Gorji and Cheng, and Goel and Chao shear force for story *i* is obtained as [18,22,23]:

$$F_i = (\beta_i - \beta_{i+1})F_n : i = n \rightarrow \beta_{n+1} = 0 \quad (1)$$

F_n which Lateral forces in story n:

$$F_n = V\left[\frac{(W_n h_n)}{\sum_{j=1}^{n}(W_j h_j)}\right]^{0.75T^{-0.2}} \quad (2)$$

$$\beta_i = \frac{V_i}{V_n} = \left[\frac{\sum_{i=1}^{n}(W_j h_j)}{(W_n h_n)}\right]^{0.75T^{-0.2}} \quad (3)$$

To develop an optimal design based on PBPD, it is required to control the interstory drift. An efficient member-yielding mechanism during push loading is necessary to achieve the target drift [24]. Figure 1 illustrates the amount of work required for an input energy of $E = \frac{1}{2}MS_V^2$ in a single-degree-of-freedom (SDOF) system [25].

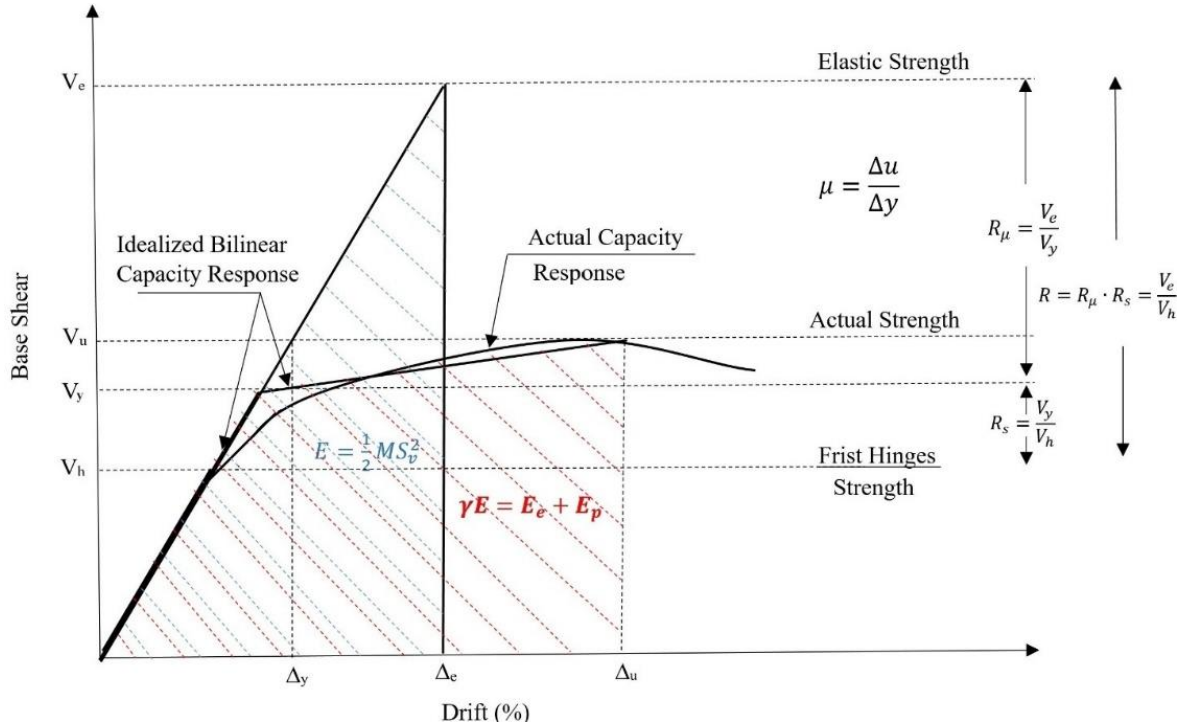

Fig. 1. Idealized structural response and energy equilibrium concept [26].

The design base shear, period-dependent dimensionless coefficient λ, and the modification factor γ dependent on the ductility factor ($\mu_s = \Delta_u/\Delta_y$) and ductility reduction factor ($R_\mu = V_e/V_y$) are calculated as [18,22,23]:

$$\frac{V}{W} = \frac{(-\lambda + \sqrt{\lambda^2 + 4\gamma S_a^{\,2}})}{2} \quad (4)$$

$$\gamma = \frac{(2\mu_s - 1)}{R_\mu^2} \quad (5)$$

$$\lambda = [\sum_{i=1}^{n}(\beta_i - \beta_{i+1})h_i] \times \left[\frac{(W_n h_n)}{\sum_{j=1}^{n}(W_j h_j)}\right]^{0.75T^{-0.2}} \times \left[\frac{\theta_p 8\Pi^2}{T^2 g}\right] \quad (6)$$

$$\gamma = \frac{(2\mu_s - 1)}{R_\mu{}^2} \tag{7}$$

This study also adopted the model of Moradifar et al. [24] to obtain the ductility and force reduction factor (R-μ-T):

$$R = -0.5 + 1.5\mu^{(-0.427-0.036\alpha+0.078\beta+T^{0.08})} \tag{8}$$

where α (post-yield slope of the system) and β (yield stress ratio) are (α=0.02 and β=1.5) [24,25],

2.2. Initial design

The web plate thickness, the beams of stories, and coupling beams are set to resist loads exerted on the stories. Therefore, the webs of the beams and columns are assumed once the steel plate thickness has been determined. To design the coupled SPSW with the two-side connections, 85% of the lateral load would be applied to the plate, while the remaining 15% would be resisted by the rest of the frame to optimize the performance of the coupling beam. Then, the design web plate force of each story (Pi) would be determined using Eq. (8) for the uncoupled SPSW and Eq. (9) for the coupled SPSW. Once the design force of the web plate in each story had been obtained, the flat web plate thickness would be calculated via Eq. (10), and the wavy trapezoidal web plate thickness was obtained using Eq. (11) – the web plate thickness estimation parameters in PBPD are shown in Table 2 [8,9].

Table 2. PBPD web plate thickness estimation parameters.

Parameter	Description
F_i	Force in each story
h_i	Story height from the base elevation
θ_p	Plastic drift
M_{pc}	Plastic moment capacity in the column base
M_{pbi}	Beam plastic moment capacity in story *i*
M_{pcbi}	Coupling beam plastic moment capacity in story *i*
h_{si}	Story height

$$(\sum_{i=1}^{n} F_i h_i)\theta_p = 2M_{pc}\theta_p + 2\sum_{i=1}^{n} M_{pbi}\theta_p + \sum_{i=1}^{n} P_i h_{si}\theta_p \tag{9}$$

$$\frac{P_i}{2} = 0.42F_y t_w L_{cf}\, sin(2\alpha) \tag{10}$$

$$\frac{P_i}{2} = 0.5F_y t_w L[1 - \frac{tan\,\theta}{\frac{L}{H}}]\, sin(2\theta_t)(1 - \frac{tan\,\theta_r}{tan\,\theta_t}) \tag{11}$$

Beam and column design

PBPD sizes the story beams and beams such that they yield at the same time or after the web plate. Moreover, beam yielding should not exceed the states defined for performance levels in FEMA (2000). The columns are designed based on the yield capacity of coupling beams and the forces exerted on the columns in the coupled shear wall [27].

2.3. Models

Borello and Fahnestock proposed a formulation to evaluate strength and the degree of coupling [8]:

$$DC = \frac{M_{coup}}{M_{total}} = \frac{M_{coup}}{M_{coup}+\sum M_{Pier}} \quad ,M_{coup} = \frac{2M_{P(CB)}}{e}(L+e) \tag{12}$$

Furthermore, the mechanism and behavior of coupled SPSWs were analytically studied. Table 3 and Figure 2 show the parameters of the model of Borello and Fahnestock [8].

Table 3. Degree of coupling parameters.

Parameter	Description
DC	Degree of coupling
M_{coup}	Coupling moment
M_{Pier}	SPSW plate and pier moment
M_{total}	Total moment
L	Length of coupling beam(CB)
e	Length of Horizontal Boundary Elements(HBE)

Borello and Fahnestock validated this mechanism for coupled SPSWs via numerical analyses on fourteen models. Figure 2 depicts the internal force diagram of a coupled SPSW in the first story [9].

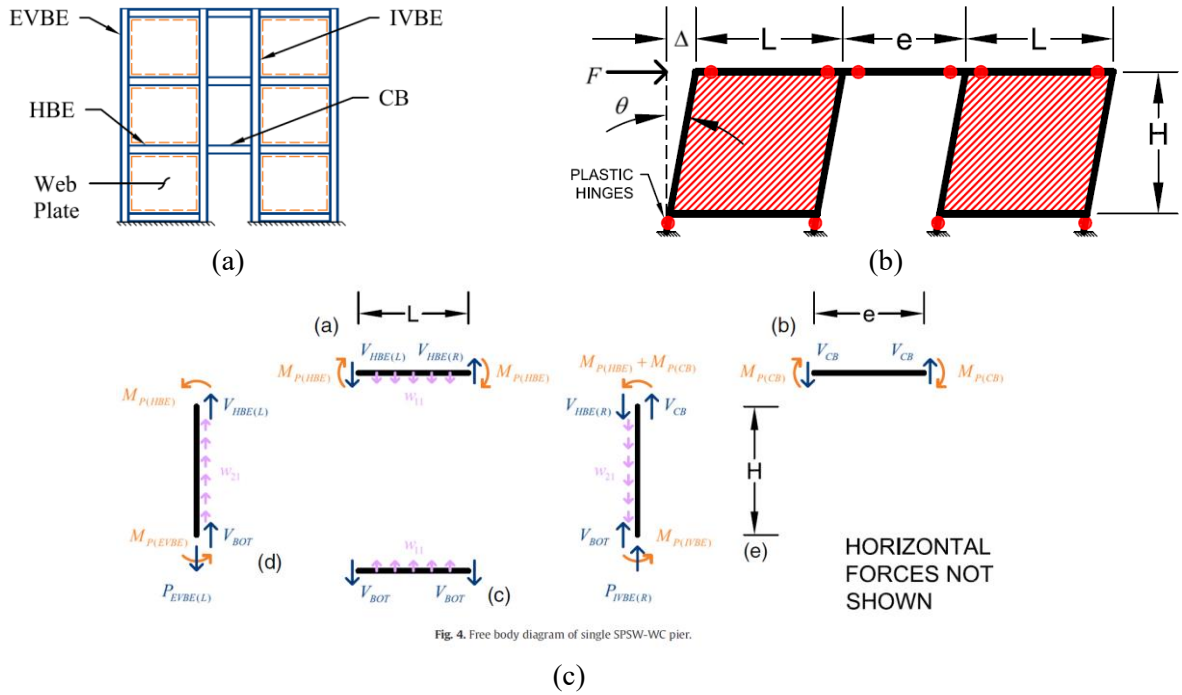

Fig. 2. a) Elevation of SPSW-WC. b) Free body diagram of single story SPSW-WC. c) Free body diagram of single story SPSW-WC. [8]

The design plate thickness is often small, and multiple techniques have been introduced to avoid the buckling of the steel plate. It was later revealed that a thinner steel plate would buckle under a small lateral load, leading to the formation of a tension field and a lateral-resisting effect. Conventional design methods use a plate thickness larger than the design thickness. This increases the cross-sectional areas of boundary elements. The steel plate is connected to the frames through two- or four-side connections. In the four-side connection, the force arising from the tension field is a flexural or axial force on the vertical boundary elements [3]. To minimize the effects of these forces on boundary elements, an LYS steel plate is employed. The SPSW consists of two flat plates

interconnected by a coupling beam. This provides architectural and material productivity advantages. Coupled SPSWs possess high seismic performance and a high degree of indeterminacy.

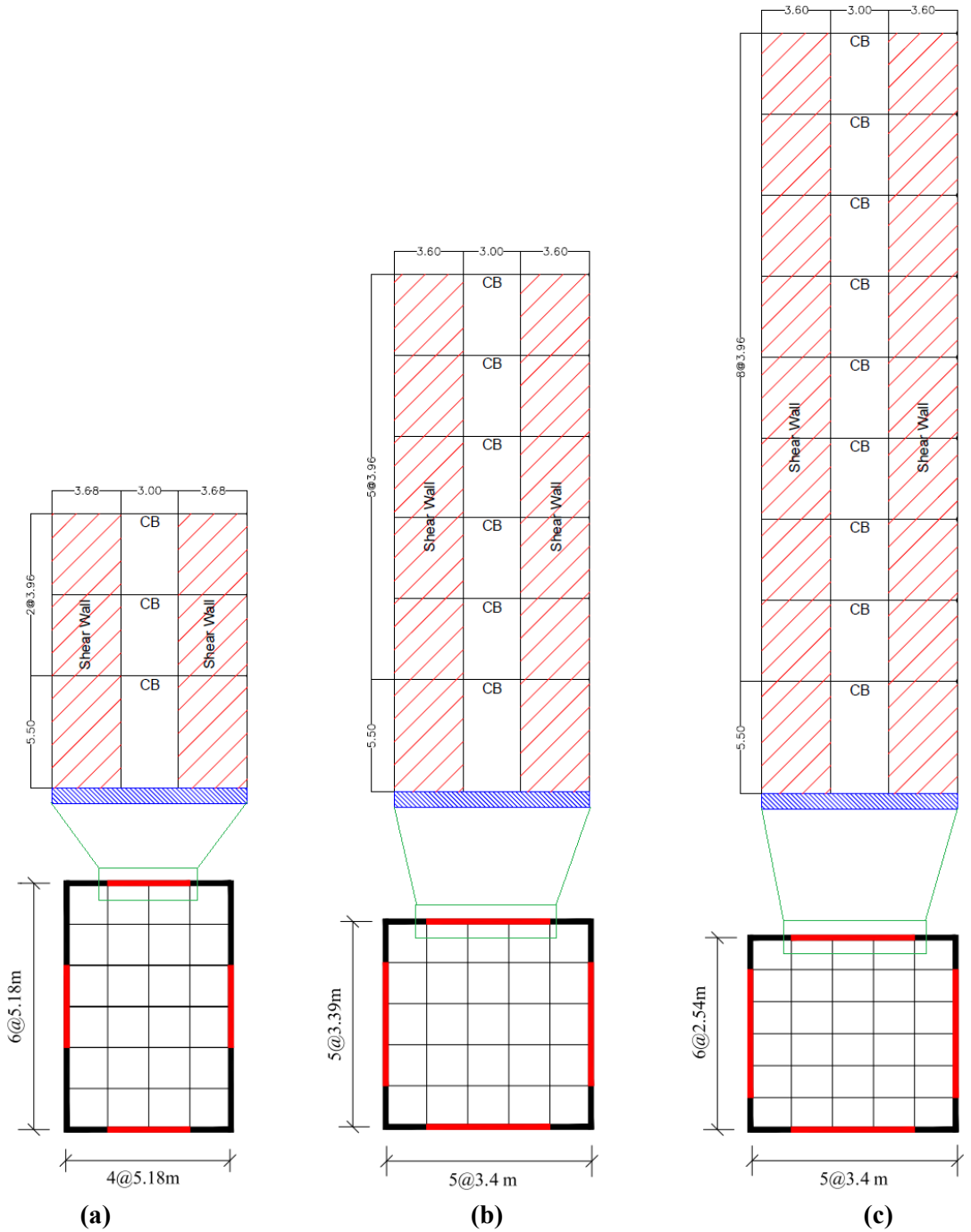

Fig. 3. Plan and Elevation view of the specimens.

Three models with three, six, and nine stories were designed based on PBPD and standard geometry under FEMA P-695, as shown in Fig. 3 [28]. Four SPSWs were assumed, given the building plan. The building was assumed to be located in Los Angeles, California, on a site with a type-D soil. Borello et al. [7–9] defined three types of coupling to define beam-coupled SPSWs based on the plastic section moduli of the coupling beam and story columns: (I) if the plastic capacity ratio of the coupling beam to the column is 1 (MPCB /MPBEAM=1), the model has flexural behavior (FLEX);

if the plastic capacity ratio of the coupling beam to the column is 2 (MPCB /MPBEAM=2), the model has flexural-shear behavior (INT); and, if the plastic capacity ratio of the coupling beam to the column is 4 (MPCB /MPBEAM=4), the model has pure shear behavior (SHEAR). This study evaluated the behavior of three-, six-, and nine-story SHEAR, INT, and FLEX models.

3. Modeling and validation (initial coupled SPSW design)

3.1. Modeling techniques

Two techniques were adopted to simulate the steel plate:

(I) Continuous model: the continuous model assumes the steel plate as a shell element. Thorburn et al. [1] proposed another model, which was employed using shell elements for the shear wall and solid elements for the coupling beam and other beams, columns, and boundary elements in ABAQUS.

(II) Strip model: The strip model uses a minimum of ten strips to simulate the steel plate. An increase in the number and angle of strips improves model accuracy. This approach was implemented in OpenSees for seismic evaluation. The beams, columns, coupling beam, and boundary elements would be simulated using the dispBeamColumn element with fiber sections. Truss elements with pure tensile materials (uniaxialMaterial ElasticPPGap) were used to model the shear wall. In addition, high-stiffness elastic elements were utilized to model leaning columns [29].

3.2. Validation

FEM software is required to more accurately evaluate a coupled SPSW. Structures are numerically modeled in such software packs, and the outputs are exploited. ABAQUS and OpenSees are used in the present work for numerical analysis. The model is validated using comparison to Choi et al. [23] (see Table 4).

Table 4. Mechanical properties of the components [23].

Material (Coppen Test)	Yield Point (MPa)	Ultimate Strength (MPa)
Infill plate	299	372
Beam web	377	527
Beam flange	353	538
Column	348	522
Link plate	407	556

Figure 4 shows the experimental model (FSPW5) model of Choi et al. [23]. Three numerical models with different configurations were simulated, evaluating the effects of the coupling beam. Pushover, cyclic, and time-history analyses were carried out to evaluate the seismic behavior and performance of different systems. The cyclic loads in cyclic analysis were set based on ATC-24 [30].

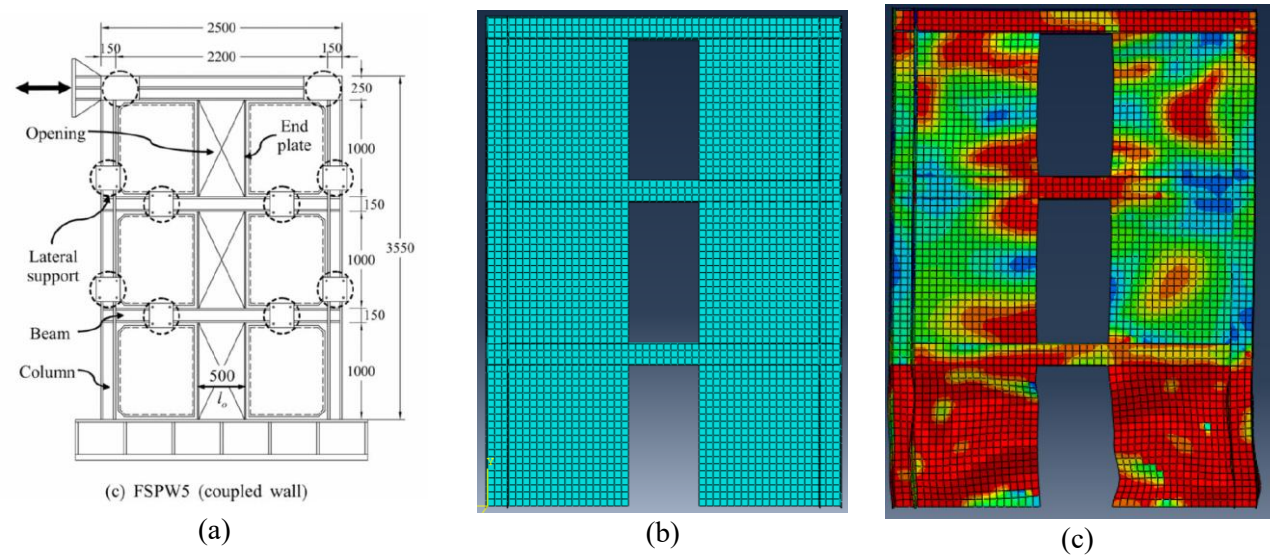

a) Experimental Model, b)Mesh model in Abaqus, c) Stress contours shape after applying cyclic load
Fig. 4. Experiential coupled SPSW Model [31].

Table 5 shows the cross-sections used in validation.

Table 5. Sections in validation [31].

Story	Steel Plate (mm)	Horizontal Boundary Element	Coupling Beam	Vertical Boundary Element
1	4	H150X100X12X20	H150X100X12X20	H-150-150X22X22
2	4	H150X100X12X20	H150X100X12X20	H-150-150X22X22
3	4	H-250X150X12	H-250X150X12	H-150-150X22X22

According to Figure 5, it is evident that the accuracy of the software and numerical modeling closely resembles that of the experimental model, including the initial stiffness, which represents the system stiffness and is almost identical to the experimental model. Although there is some difference in yielding, the value estimated by the software model is slightly lower than that of the experimental model. On the other hand, in higher loops, the return slope is somewhat steeper than the experimental model, likely due to certain idealizations (in modeling, materials, etc.). By the way, the energy dissipation, represented by the area under a loop of the system, is similar to the experimental model. Overall, the results of the software modeling are reliable and closely aligned with the real model, indicating the validity of the modeling process.

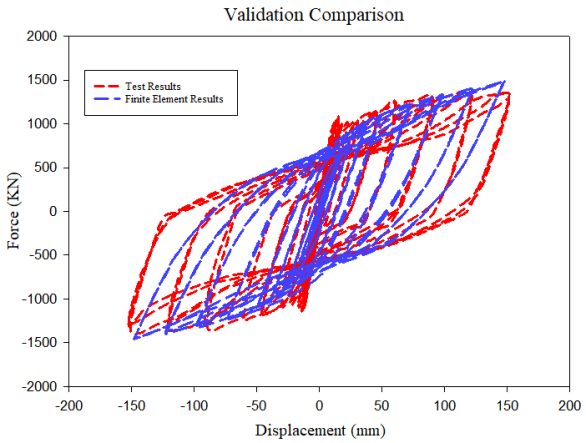

Fig. 5. Experimental versus numerical hysteresis loops.

3.3. Modeling

As mentioned, ABAQUS, SAP2000, and OpenSees were employed to simulate the 3-, 6-, and 9-story SPSWs. Tables 6-8 provide the cross-sections in structures. For initial design, coupled SPSW plates were simulated as tensile strips in SAP2000. To develop two-side connections, beam-to-beam strips were developed, as shown in Fig. 6. Thorburn et al. used a strip model in which strips are connected over a length of L_p (Eq. (13)). This equation is dependent on the plate size and assumed angle [1]. The area of each strip is found using Eq. (14), where A_s and n_s denote the area and number of strips, respectively [9].

As mentioned, ABAQUS, SAP2000, and OpenSees were employed to simulate the three-, six-, and nine-story SPSWs. Tables 6-8 provide the cross-sections in structures. For initial design, coupled SPSW plates were simulated as tensile strips in SAP2000. To develop two-side connections, beam-to-beam strips were developed, as shown in Fig. 6. Thorburn et al. used a strip model in which strips are connected over a length of Lp (Eq. (13)). This equation is dependent on the plate size and assumed angle [1]. The area of each strip is found using Eq. (14), where As and ns denote the area and number of strips, respectively [9].

$$L_p = L - H\tan\theta = L(1 - \frac{tan(\theta)}{L/H}) \tag{13}$$

$$A_s = (t_w L_p \cos\theta)/n_s = t_w L\left(1 - \frac{\tan(\theta)}{L/H}\right)\cos\theta\,/n_s \tag{14}$$

To improve accuracy in the model, it is required to use a large number of strips and precise angles. Modified strip model, building on the work of Thorburn et al., incorporates bilinear flexural and axial hinges, a diagonal compression strut, and deterioration behavior to capture key phenomena observed in experimental studies. This model effectively simulates the inelastic pushover response of SPSWs, including base shear capacity, column and beam demands, and energy dissipation mechanisms [1].

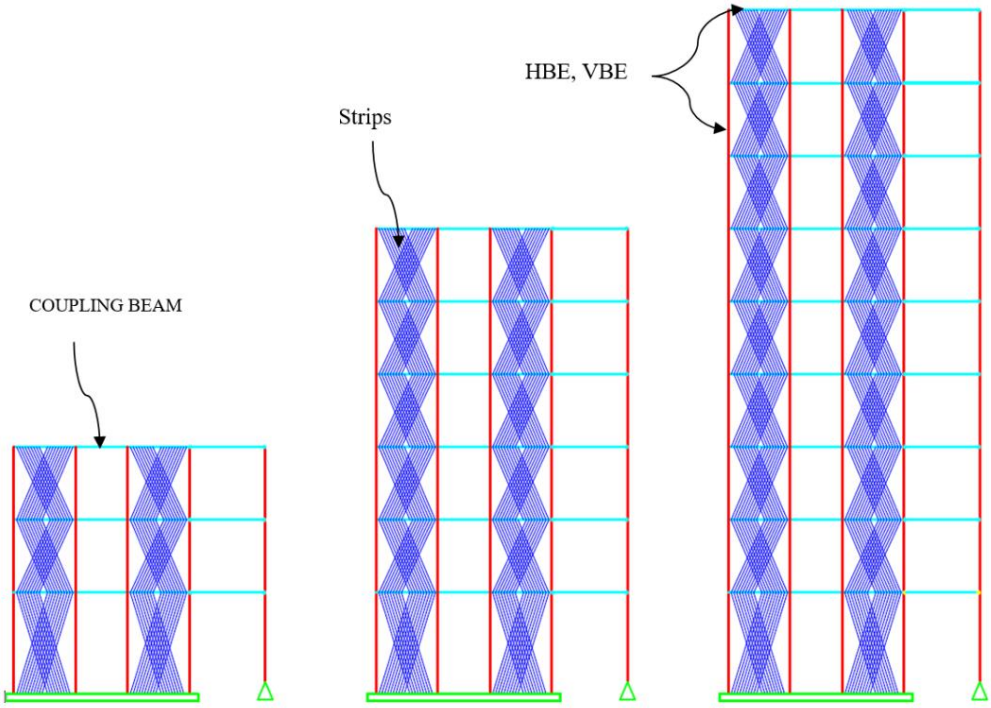

Fig. 6. Frame models in SAP2000.

Table 6. Sections of 3-story models.

FRAME	STORY	BEAM	COUPLING-BEAM	COLUMN-EXTERNAL	COLUMN-INTERNAL	PLATE(mm)
SHEAR	3	W10X15	W10X54	W12X58	W12X65	1
	2	W10X15	W10X54	W12X58	W12X65	1.6
	1	W10X15	W10X54	W12X58	W12X65	2.2
INT	3	W12X14	W12X14	W12X45	W12X87	1
	2	W12X14	W12X14	W12X45	W12X87	1.6
	1	W12X14	W12X14	W12X87	W12X87	2.2
FLEX	3	W10X15	W12X19	W12X45	W12X53	1
	2	W10X15	W12X19	W12X45	W12X53	1.6
	1	W10X15	W12X19	W12X53	W12X53	2.2

Table 7. Sections of 6-story models.

FRAME	STORY	BEAM	COUPLING-BEAM	EXTERNAL-COLUMN	INTERNAL-COLUMN	PLATE(mm)
SHEAR	6	W12X22	W12X79	W14X61	W14X90	2.1
	5	W12X22	W12X79	W14X61	W14X90	3.4
	4	W14X22	W14X82	W14X90	W14X90	4.3
	3	W14X22	W14X82	W14X90	W14X90	5.5
	2	W14X30	W14X109	W14X120	W14X145	5.5
	1	W14X30	W14X109	W14X120	W14X145	6.5
INT	6	W14X22	W14X22	W14X61	W12X65	2.1
	5	W14X22	W14X22	W14X61	W12X65	3.4
	4	W14X22	W14X22	W12X170	W12X106	4.3
	3	W14X22	W14X22	W12X170	W12X106	5.5
	2	W14X30	W14X30	W12X230	W12X106	5.5
	1	W14X30	W14X30	W12X230	W12X230	6.5
FLEX	6	W10X19	W14X22	W14X61	W12X65	2.1
	5	W10X19	W14X22	W14X61	W12X65	3.4
	4	W10X19	W14X22	W12X170	W12X106	4.3
	3	W10X19	W14X22	W12X170	W12X106	5.5
	2	W12X22	W14X30	W12X230	W12X106	5.5
	1	W12X22	W14X30	W12X230	W12X230	6.5

Modeling Details:

- Element Types: Shell elements represented steel plates in ABAQUS, while truss elements modeled tension-only behavior in OpenSees. DispBeamColumn elements with fiber sections were employed for beams and columns to capture nonlinear flexural behavior.
- Boundary Conditions: Fixed supports were applied at column bases, while rigid diaphragm constraints were used to model floor behavior. Elastic rigid beams connected to leaning columns ensured accurate mass distribution and seismic load transfer.
- Material Properties: Yield and ultimate strengths for steel plates, coupling beams, and boundary elements were defined based on experimental data (Table 4). High-strength materials were employed for coupling beams to optimize energy dissipation under seismic loading.

3.4. Records

Accelerograms representing strong ground motion were selected based on FEMA P-695 guidelines and relevant studies. Table 9 lists the far-field records used in this study, which were scaled according to the ASCE07-10 methodology[32–34].

Table 8. Sections of 9-story models.

FRAME	STORY	BEAM	COUPLING-BEAM	EXTERNAL-COLUMN	INTERNAL-COLUMN	PLATE(mm)
SHEAR	9	W16X31	W18X55	W18X71	W18X60	2.2
	8	W16X31	W18X55	W18X71	W18X60	3.5
	7	W16X50	W18X76	W18X97	W18X86	4.6
	6	W16X50	W18X76	W18X97	W18X86	5.5
	5	W16X57	W18X97	W18X175	W18X119	6.5
	4	W16X57	W18X97	W18X175	W18X119	6.7
	3	W18X46	W18X97	W24X146	W24X131	7.1
	2	W18X46	W18X97	W24X146	W24X131	7.4
	1	W18X46	W18X97	W24X192	W24X131	8.4
INT	9	W16X31	W16X31	W18X55	W18X86	2.2
	8	W16X31	W16X31	W18X55	W18X86	3.5
	7	W16X50	W16X50	W18X76	W18X97	4.6
	6	W16X50	W16X50	W18X76	W18X97	5.5
	5	W16X57	W16X57	W18X76	W24X131	6.5
	4	W16X57	W16X57	W18X143	W24X131	6.7
	3	W18X46	W18X46	W18X143	W24X131	7.1
	2	W18X46	W18X46	W24X192	W24X162	7.4
	1	W18X46	W18X46	W24X192	W24X162	8.4
FLEX	9	W10X19	W10X68	W14X61	W12X65	2.2
	8	W10X19	W10X68	W14X61	W12X65	3.5
	7	W10X19	W10X68	W14X61	W12X65	4.6
	6	W10X19	W10X68	W14X61	W12X65	5.5
	5	W10X19	W10X68	W14X61	W12X65	6.5
	4	W10X19	W10X68	W12X170	W12X106	6.7
	3	W10X19	W10X68	W12X170	W12X106	7.1
	2	W12X22	W12X79	W12X170	W12X106	7.4
	1	W12X22	W12X79	W12X170	W12X230	8.4

This study focuses on far-field ground motion effects using FEMA P-695 records scaled according to ASCE 7-10 provisions. While near-fault effects represent a critical area of study, they fall outside the scope of this research. The generalized findings here are intended to inform the seismic performance of coupled SPSWs in regions with far-field seismic characteristics.

4. Results and discussion

Since SPSWs have almost the same behavior in the strip model approach as braced frames and Takeda model, the failure limits of FEMA 356 were adopted in the present work. FEMA 356 defines immediate occupancy (IO), life safety (LS), and collapse prevention (CP) limits as follows [35]:

(i) IO limit: the FEO hazard level cannot occur in failed beams and columns under the earthquake, while slight buckling in beams and slight distortion in the SPSW wall are allowable in the condition that connections are intact.

(ii) LS limit: failed beams and columns cannot undergo the DBE level, with relatively large buckling in beams and columns and relatively large distortion and yielding in the SPSW plate, while many of the connections have failed.

(iii) CO limit: the structure experiences the MCE level in massively failed beams and columns, with remarkably large buckling and distortions in the SPSW plate, most connections failing, and the structure collapsing.

Table 9. Events and records from selected earthquakes FEMA p695 with details [34].

No.	Name Record	Station Name	Year	Mw	Epicentral Distance	Soil Type	Fault Type	PGA (g)	PGV (cm/s)	Source
1	Northridge	Beverly Hills-Mulholland	1994	6.7	13.3	D	Thrust	0.52	63	USC
2	Northridge	Canyon Country-WLC	1994	6.7	26.5	D	Thrust	0.48	45	USC
3	Duzce, Turkey	Bolu	1999	7.1	41.3	D	Strike-slip	0.82	62	ERD
4	Hector Mine	Hector	1999	7.1	26.5	C	Strike-slip	0.34	42	SCSN
5	Imperial Valley	Delta	1979	6.5	33.7	D	Strike-slip	0.35	33	UNAMUCSD
6	Imperial	El Centro Array #11	1979	6.5	29.4	D	Strike-slip	0.38	42	USGS
7	Kobe, Japan	Nishi-Akashi	1995	6.9	8.7	C	Strike-slip	0.51	37	CUE
8	Kobe, Japan	Shin-Osaka	1995	6.9	46	D	Strike-slip	0.24	38	CUE
9	Kocaeli, Turkey	Duzce	1999	7.5	98.2	D	Strike-slip	0.36	59	ERD
10	Kocaeli, Turkey	Arcelik	1999	7.5	53.7	C	Strike-slip	0.22	40	KOERI
11	Landers	Yermo Fire Station	1992	7.3	86	D	Strike-slip	0.24	52	CDMG
12	Landers	Coolwater	1992	7.3	82.1	D	Strike-slip	0.42	42	SCE
13	Loma Prieta	Capitola	1989	6.9	9.8	D	Strike-slip	0.53	35	CDMG
14	Loma Prieta	Gilroy Array #3	1989	6.9	31.4	D	Strike-slip	0.56	45	CDMG
15	Manjil, Iran	Abbar	1990	7.4	40.4	C	Strike-slip	0.51	54	BHRC
16	Superstition Hills	El Centro Imperial. Co.	1987	6.5	35.8	D	Strike-slip	0.36	46	CDMG
17	Superstition Hills	Poe Road (temp)	1987	6.5	11.2	D	Strike-slip	0.45	36	USGS
18	Cape Mendocino	Rio Dell Overpass	1992	7	22.7	D	Thrust	0.55	44	CDMG
19	Chi-Chi, Taiwan	CHY101	1999	7.6	32	D	Thrust	0.44	115	CWB
20	Chi-Chi, Taiwan	TCU045	1999	7.6	77.5	C	Thrust	0.51	39	CWB
21	San Fernando	LA-Hollywood Stor	1971	6.6	39.5	D	Thrust	0.21	19	CDMG
22	Friuli, Italy	Tolmezzo	1976	6.5	20.2	C	Thrust	0.35	31	--

FEMA P-356 and SEAOC (1995) standards and earlier works proposed maximum allowable drifts of 0.5%, 2.5%, and 5% for the FOE, DBE, and MCE levels for IO, LS, and CP limits in braced frame systems, respectively. The maximum allowable residual drift is 0.2%, 1%, and 4% for FOE, DBE, and MCE levels, as shown in Table 10 [35–37].

Table 10. Performance levels for SPSWs [35].

Elements	Parameter	Structural Performance Levels		
		CP	LS	IO
SPSW	Drift	5%	2.5%	0.5%
	Res. Drift	4%	1%	0.2%

4.1. Pushover analysis

Pushover analysis was performed on the SPSW models. First, the initial hinges formed at the end of the column bases i.e., the column base ends were the first lateral load-resisting elements. Then, the steel plates began to form hinges. Considering the tension field forming in the plate and two-side plate connections (the steel plate is not connected to the column web), hinge formation began at the corner and propagated diagonally. Then, plastic hinges formed at the end of the beams that are connected to the coupled beams and the plate. The pushover curves were bilinearized for a design drift of 2% using the Young method for a better comparison of the models [38].

Figure 7 compares the pushover curves of the three-, six-, and nine-story SPSW models. As can be seen, the INT and SHEAR three-story models had 28% and 25% higher stiffness than the FLEX three-story model in the first elastic phase. Once the SPSW exceeded the elastic region, the coupling effect and plastic behavior became significant. The ductility factors of the INT and SHEAR models were 12% and 5% higher than that of the FLEX model, and the INT and SHEAR models had 2% and 8% larger overstrength factors than the FLEX model. This suggests that the INT and SHEAR three-story models outperformed the FLEX three-story model in the plastic region and provided larger load capacities.

In the first elastic phase, the INT and SHEAR six-story models had 13% and 15% higher initial stiffness than the FLEX six-story model, respectively. In the plastic region, the coupling effect and plastic behavior became prominent. The INT and SHEAR models had a 2% higher and a 6% lower ductility factor than the FLEX model, respectively. The INT and SHEAR models also had 12% and 3% smaller overstrength factors than the FLEX model. As a result, the INT and SHEAR six-story models showed lower plastic performance than the FLEX model and required modification.

The INT and SHEAR nine-story models showed 71% and 99% higher initial stiffness than the FLEX nine-story model in the elastic phase. In the plastic phase, the coupling effect and plastic behavior became significant, and the INT and SHEAR models had 9% larger ductility factors than the FLEX model. The INT and SHEAR models also had 7% and 6% smaller overstrength factors than the FLEX model, respectively. Thus, the INT and SHEAR nine-story models had almost the same plastic performance as the FLEX nine-story model.

Overall, the SHEAR model outperformed the FLEX and INT models. All result for Pushover analysis is shown in below table 11.

Table 11. Result for Pushover analysis.

	Flex			int			shear		
	9St	6St	3St	9St	6St	3St	9St	6St	3St
Rs	1.50	1.41	1.31	1.39	1.24	1.34	1.42	1.37	1.41
Rμ	2.20	2.94	3.00	2.40	3.01	3.35	2.39	2.77	3.16
R	3.30	4.14	3.93	3.35	3.74	4.49	3.39	3.78	4.47
μ	2.85	4.44	4.33	3.19	4.57	5.18	3.13	3.80	4.42
K0=KE (kN/mm)	47.67	59.43	20.77	81.71	67.22	26.64	94.75	68.34	25.03

2.4. Cyclic analysis

Cyclic analysis was carried out on the SPSWs. Cyclic analysis is an analytical method that is used to evaluate the behavior of structures under repeating and variable loads.

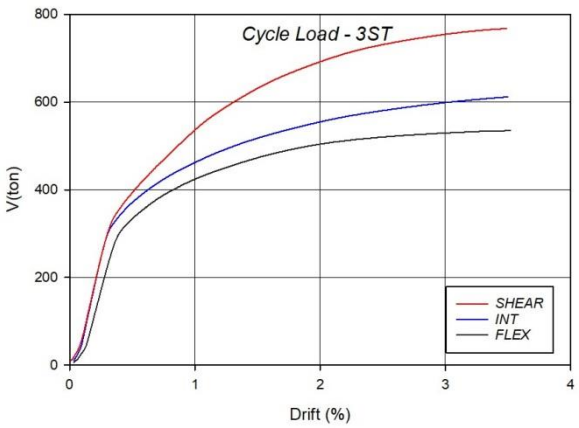

(a) 3-story SPSW

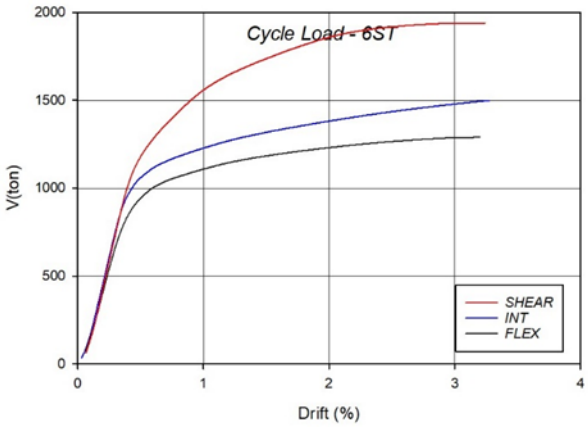

(b) 6-story SPSW

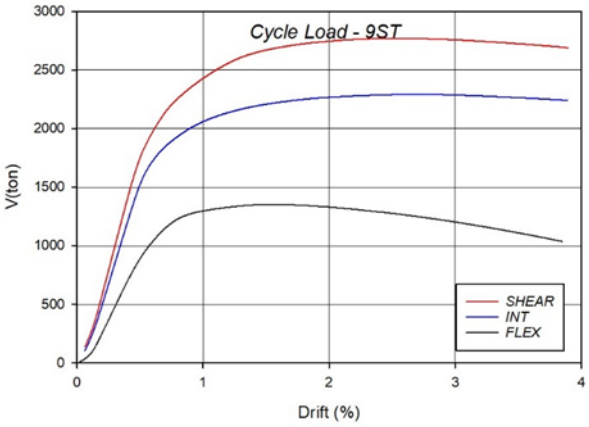

(c) 9-story SPSW

Fig. 7. Pushover curves.

Structures undergo loading-unloading cycles, measuring important parameters such as displacement, strength, and damping. Different protocols can be adopted, where the form, intensity, and number of cycles are determined. This study employed the ATC protocol as a widely used protocol in the cyclic analysis of structures. Figure 8 compares the cyclic behavior of the systems.

The analysis of the three-, six-, and nine-story models indicated that out-of-plane buckling and steel plate yielding at drifts below 1% lead to pinching in the cyclic curves. Therefore, these structures showed lower strength and damping at such drifts. As shown in Fig. 8, the FLEX model had lower stiffness than INT and SHEAR since it had a smaller coupling beam section. It can also be said that the hysteresis area of the curves, which represents cyclic damping, was smaller for FLEX than for INT and SHEAR. This is explained by the reduced coupling beam section, which led to lower energy absorption in the SHEAR model. The peaks (strength indicators) were lower for FLEX than for INT and SHEAR, suggesting that the FLEX model had a lower bearing capacity. Although the SHEAR model had almost the same stiffness as the INT model, it had higher ultimate strength than the INT model under the cyclic load. This is explained by its higher secondary slope, which implies the presence of a stronger coupling beam. A stronger coupling beam led to higher plastic strength in the SHEAR model. Furthermore, the SHEAR model with a larger unloading slope experienced a smaller residual drift. However, reliable and valid residual drift estimates could be derived from time-history analysis.

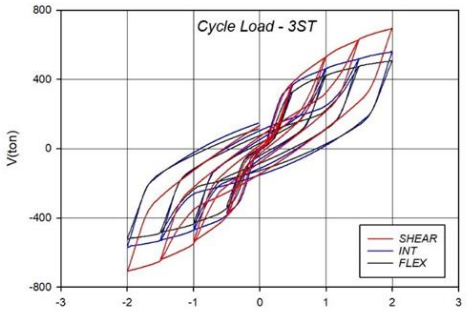

(a) 3-story SPSW

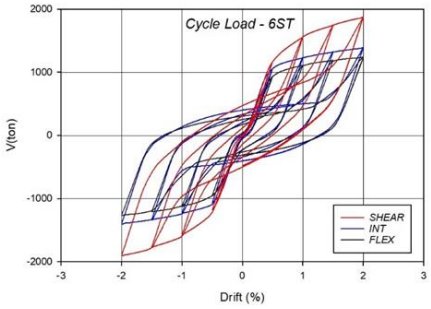

(b) 6-story SPSW

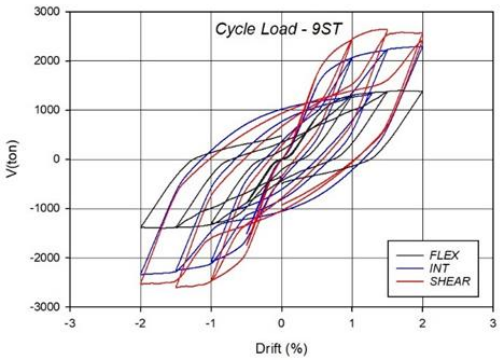

(c) 9-story SPSW

Fig. 8. Cyclic analysis curves.

4.3. Time-history analysis

Figures 9-17 plot the time-history analysis results (only the median data were used since the drift variations were excessively large or small under some earthquake records, and the mean data would not be reliable for most records).

According to Figs. 11(a) and 11(b), the FLEX and INT models experienced the largest drifts at the FOE level; the drifts exceeded the allowable drift of 0.5% for the FOE level, while the SHEAR model showed the highest performance and met the IO limit for the three-, six-, and nine-story buildings. The six-story models had almost the same maximum drift at the FOE level, with SHEAR experiencing a relatively smaller drift than INT and FLEX. However, the top stories of the six-story building (stories 3-6) in INT and FLEX models did not meet the IO limit and would require slight modifications.. All models exhibited residual drifts below 0.2%, meeting the maximum allowable residual drift criterion. As illustrated in Fig. 14, the INT and SHEAR models demonstrated superior performance compared to the FLEX model in terms of residual drift. As shown in Figs. 15-17, the INT model showed relatively lower performance than FLEX and SHEAR in terms of the maximum drift for the nine-story structure. However, all three models exceeded the IO maximum allowable drift at the FOE level. Although the INT model exhibited larger maximum drifts, its residual drifts were within acceptable limits, as shown in Fig. 17. In contrast, the SHEAR and FLEX models demonstrated comparable residual drift values. Overall, these models met the maximum allowable residual drift criterion and showed good structural performance.

At the FOE level, INT, SHEAR, and SHEAR had the highest performance in the three-, six-, and nine-story structures for the maximum drift, respectively. In terms of the residual drift, FLEX, SHEAR, and INT showed the highest performance for the three-, six-, and nine-story SPSWs,

respectively. Moreover, FLEX, INT, and SHEAR models had the lowest maximum drift performance for the three-, six-, and nine-story structures, and FLEX, INT, and INT had the lowest residual drift performance for three-, six-, and nine-story SPSWs, respectively. It can be concluded that SHEAR would outperform INT and FLEX for high-rise SPSWs, while INT would be the most effective model for low-rise structures.

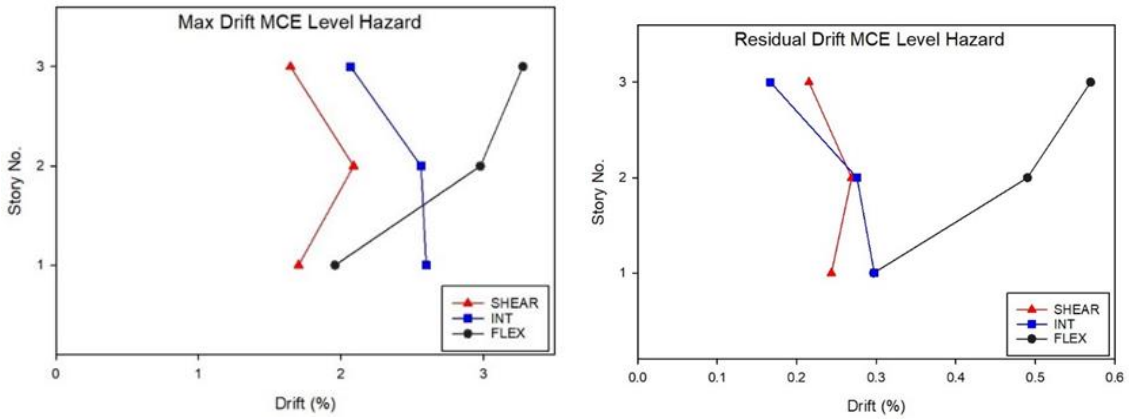

Fig. 9. Median (a) maximum drift and (b) residual drift of 3-story SPSWs at MCE level.

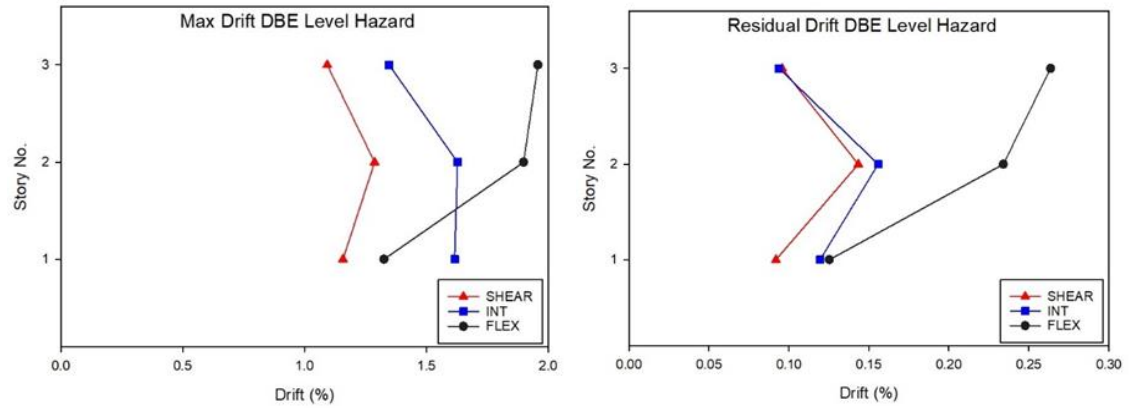

Fig. 10. Median (a) maximum drift and (b) residual drift of 3-story SPSWs at DBE level.

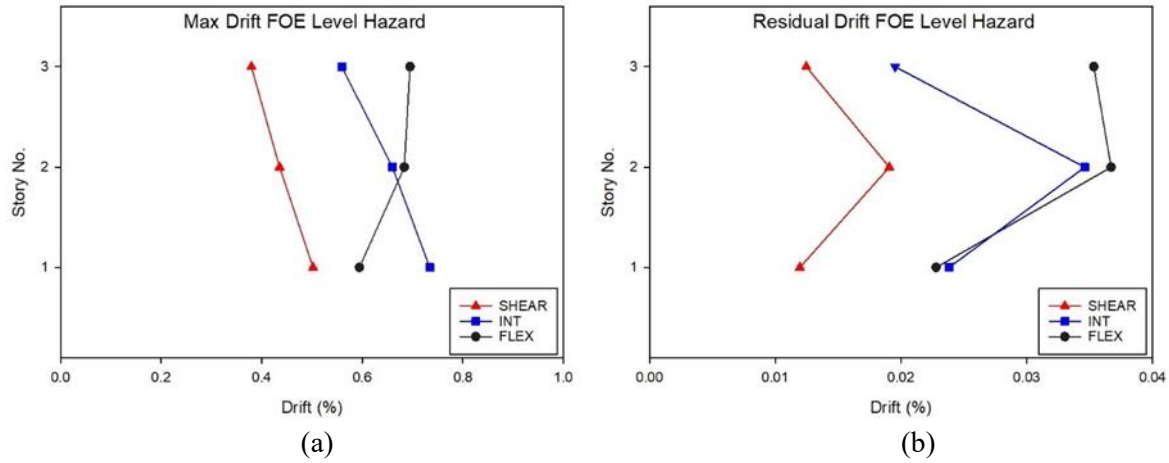

Fig. 11. Median (a) maximum drift and (b) residual drift of 3-story SPSWs at FOE level.

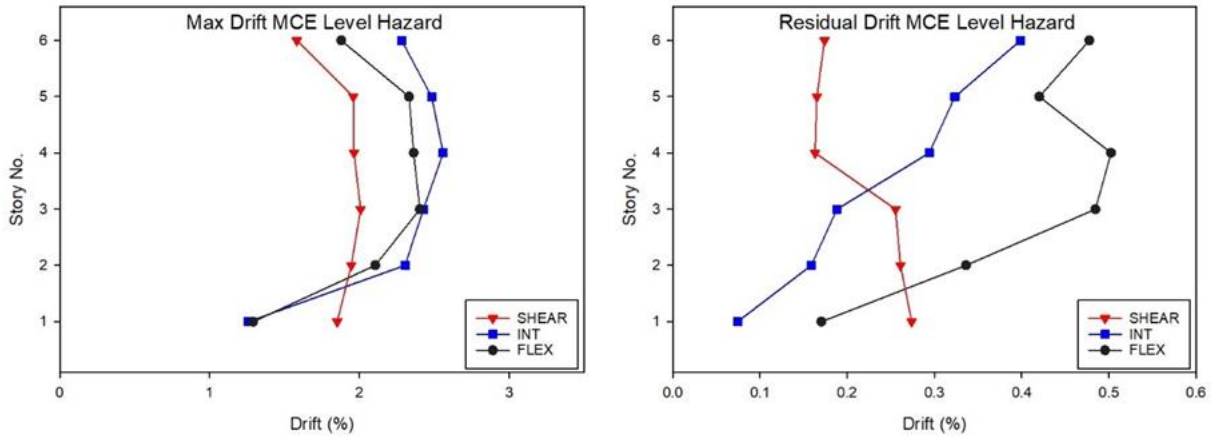

(a) (b)

Fig. 12. Median (a) maximum drift and (b) residual drift of 6-story SPSWs at MCE level.

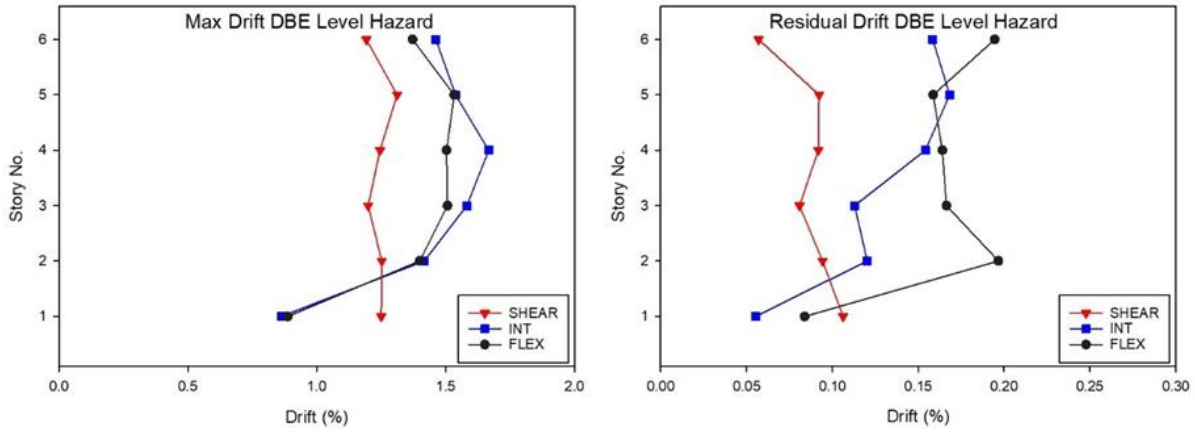

(a) (b)

Fig. 13. Median (a) maximum drift and (b) residual drift of 6-story SPSWs at DBE level.

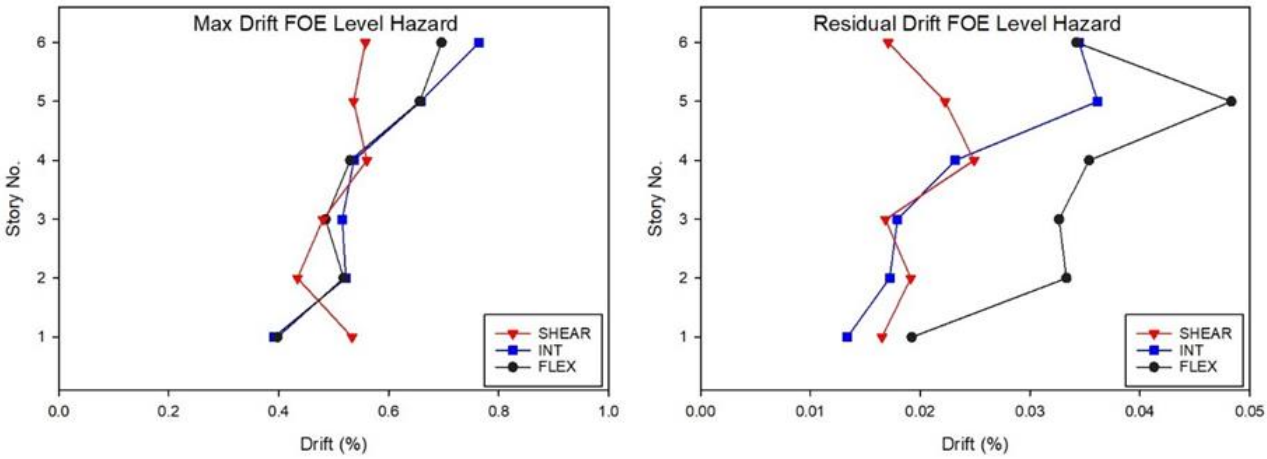

(a) (b)

Fig. 14. Median (a) maximum drift and (b) residual drift of 6-story SPSWs at FOE level.

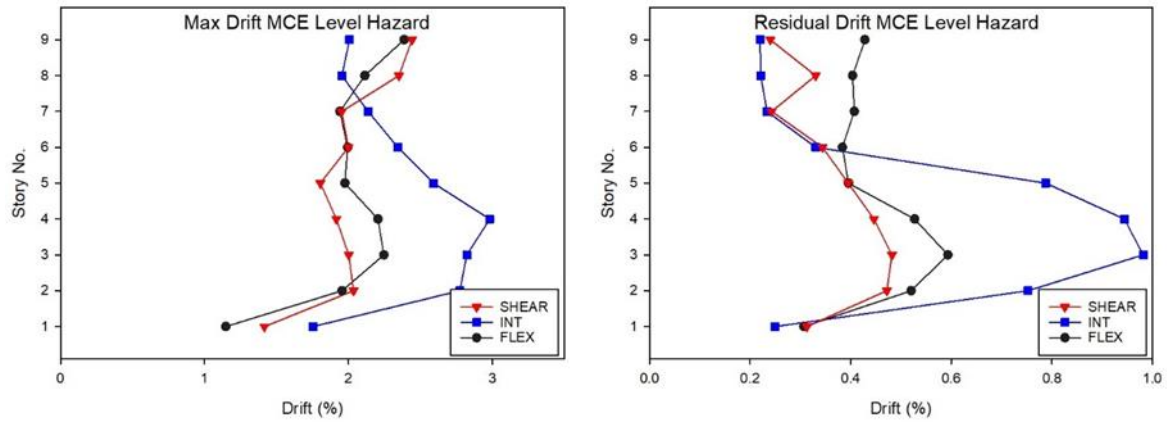

Fig. 15. Median (a) maximum drift and (b) residual drift of 9-story SPSWs at MCE level**.**

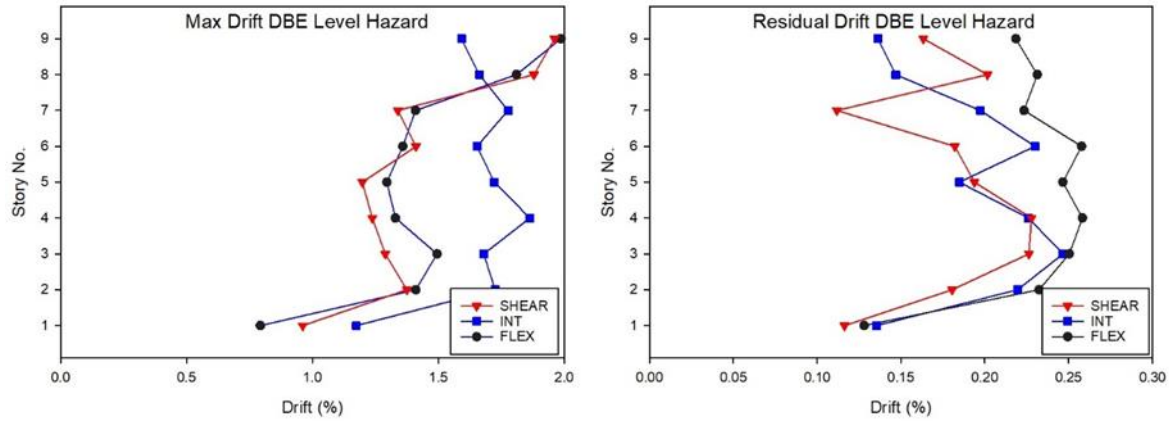

Fig. 16. Median (a) maximum drift and (b) residual drift of 9-story SPSWs at DBE level.

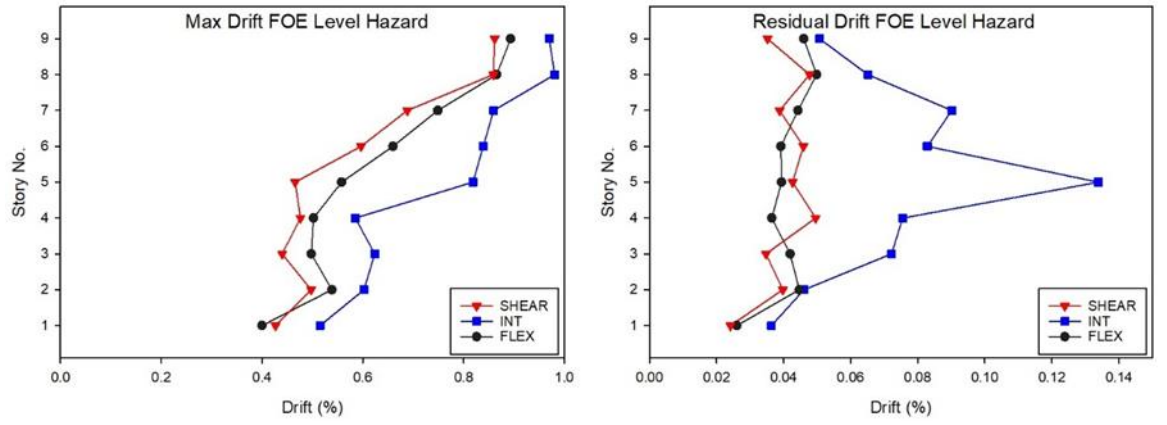

Fig. 17. Median (a) maximum drift and (b) residual drift of 9-story SPSWs at FOE level.

According to Fig. 10(a), all three SPSWs met the LS criterion at the DBE level (which is a major seismic hazard level). The SHEAR and FLEX models showed the highest and lowest performance at the DBE level (as with their performance at the FOE level), respectively. The same case holds for the residual drift; the SHEAR model outperformed INT and FLEX. The three models met the LS

criterion, with the SHEAR model outperforming INT and FLEX in terms of the maximum drift (and the FLEX had higher performance than INT). Moreover, the residual drift performance of the models was in the order of SHEAR>INT>FLEX. As shown in Fig. 16(a), the SHEAR and FLEX models had almost the same maximum drifts for the nine-story SPSWs (with SHEAR having slightly higher performance), whereas INT had the lowest maximum drift performance. Overall, all three models met the LS criterion. As shown in Fig. 16(b), the residual drift performance of the models for the nine-story SPSWs was in the order of SHEAR>INT>FLEX.

The MCE level is also a major seismic hazard level. According to Fig. 9(a), the three-story SPSW met the CP criterion; however, the INT model did not meet the LS criterion, whereas SHEAR and FLEX met the LS criterion. This is also the case with the residual drift. Overall, maximum drift and residual drift performances were in the order of SHEAR>FLEX>INT. As shown in Fig. 12(a), almost all the models met not only the CP but also LS criterion, with the SHEAR and INT models showing the highest and lowest performance, respectively. In terms of the residual drift, all the models somewhat met the CP and LS criteria, with slight damage to the SPSWs. According to Fig. 12(b), SHEAR showed excellent performance, while FLEX and INT experienced damage; the INT model had higher damage than the FLEX one and could not meet the IO criterion.

It can be concluded that SHEAR would be the optimal structural model for all three SPSWs. However, further evaluation is required to verify these findings using IDA.

4.4. IDA

IDA was proposed by Bertero and has been employed through several approaches. It was accepted by the FEMA and incorporated into FEMA 350 and FEMA 351 provisions for the overall collapse capacity measurement of structures. IDA would estimate the structural response at different seismic hazard levels and evaluate structural behavior from the linear elastic phase to the collapse phase [39,40]. Vamvatsikos and Cornell conducted multi-record analyses to obtain deep insights into the record potential level, understand rare and common ground motions, and estimate the dynamic capacity to evaluate the stability of a structure under multiple records. Their methodology was verified [41]. Figures 18-20 provide the IDA curves (where the horizontal axis represents the ID criterion that stands for the structural responses, while the vertical axis represents seismic intensity (IM or Sa)).

According to Figs. 18-20, the 50-fractile curves became flattened before the CP level. This suggests that the models could not meet the CP criterion, and SPSWs underwent full failure, while nonlinear time-history analysis demonstrated that all the models had satisfactory CP performance. As shown in Figs. 18(a)-18(c), the models met the LS and IO limits. According to Fig. 18(ad), the initial stiffness was almost the same in the three models, with a slight difference in the order of SHEAR>FLEX>INT. This is consistent with the pushover curves. As with the pushover analysis, SHEAR had a larger seismic capacity than the FLEX and INT models. However, in contrast to pushover analysis, FLEX had a greater seismic capacity than INT. This highlights the significance of IDA. As shown in Figs. 19(a)-19(c), the same case holds for the six-story SPSWs, except that FLEX and INT somewhat met the limits and had almost the same ultimate capacity, with no significant 50-fractile difference (see Fig. 19(d)). The IDA initial stiffness data were consistent with the pushover analysis. The nine-story SPSWs had the same IDA outputs as the three-story ones (see Figs. 20(a)-20(c)); the initial stiffness was in the order of SHEAR>INT>FLEX, as with the pushover analysis. The FLEX model, however, had a larger collapse capacity than the INT model.

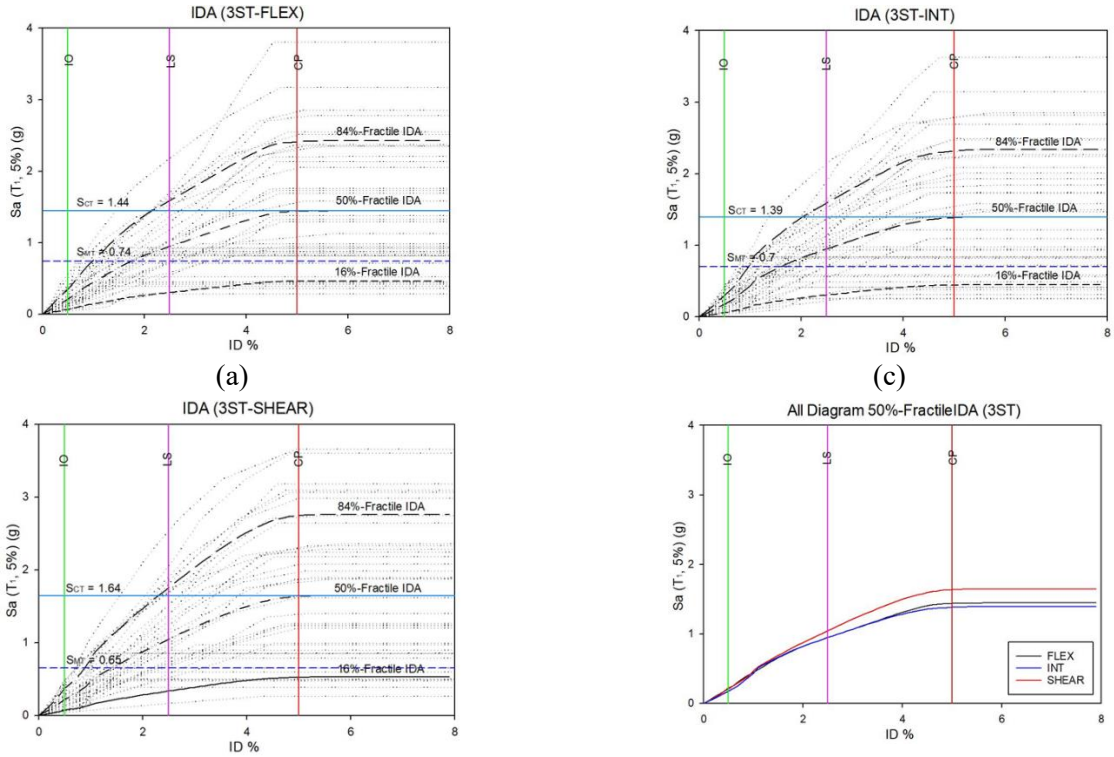

Fig. 18. IDA curves of (a) FLEX, (b) INT, and (c) SHEAR models and (d) 50-fractile comparison of 3-story SPSWs.

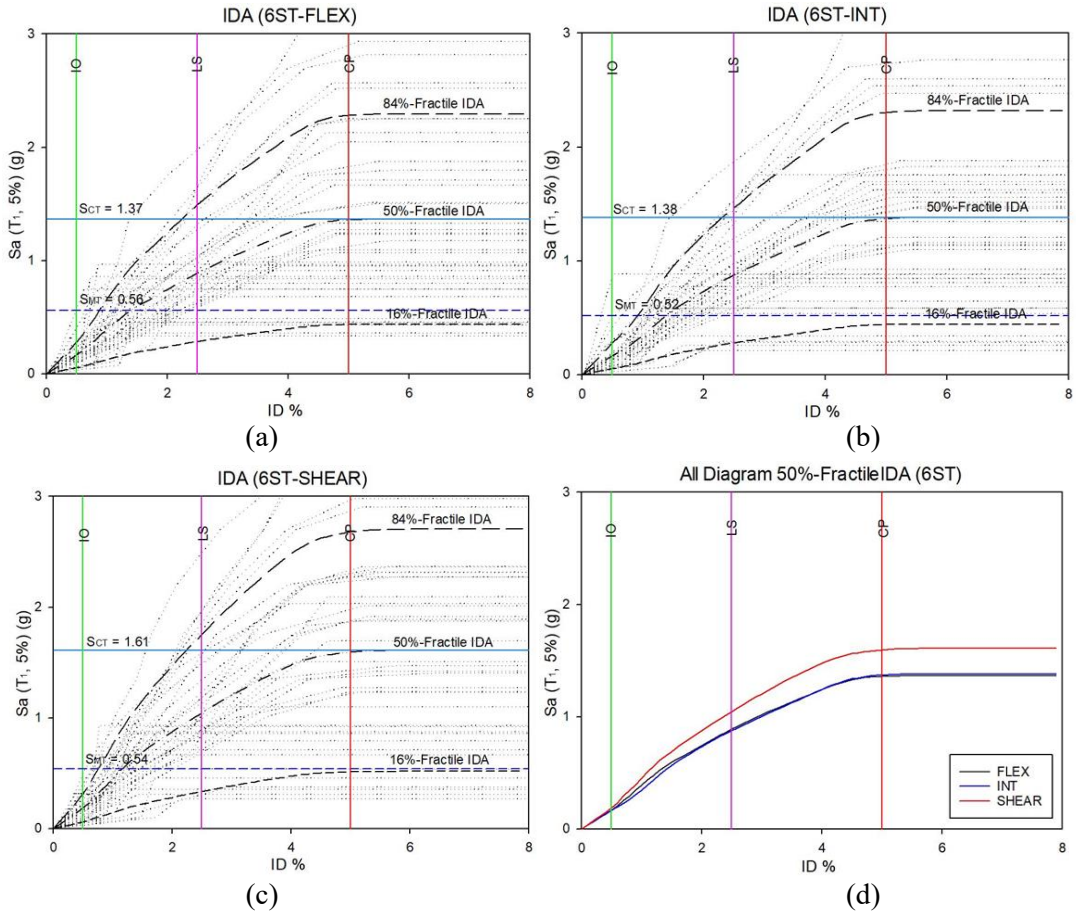

Fig. 19. IDA curves of (a) FLEX, (b) INT, and (c) SHEAR models and (d) 50-fractile comparison of 6-story SPSWs.

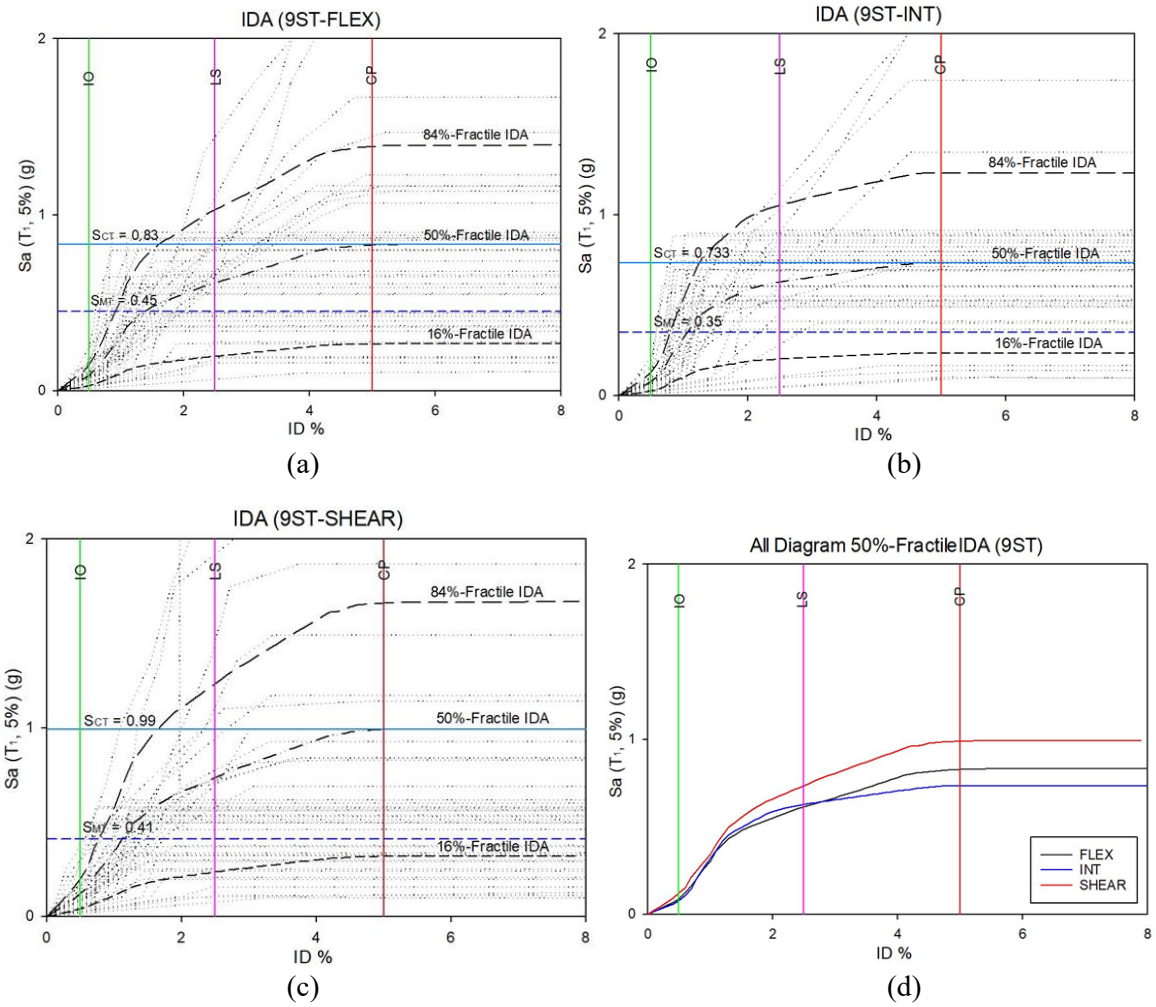

Fig. 20. IDA curves of (a) FLEX, (b) INT, and (c) SHEAR models and (d) 50-fractile comparison of 9-story SPSWs.

Table 12. Accelerations at different limit states of collapse for different models.

N-ST	Model	Sa (g)		
		IO	LS	CP
3-ST	FLEX	0.204959	0.946159	1.437385
	INT	0.220273	1.044747	1.635871
	SHEAR	0.176333	0.946688	1.380794
	Average	0.200522	0.979198	1.484683
6-ST	FLEX	0.166644	0.888363	1.35854
	INT	0.166623	0.873302	1.372087
	SHEAR	0.186258	1.044809	1.595444
	Average	0.173175	0.935491	1.442024
9-ST	FLEX	0.087946	0.61317	0.826491
	INT	0.07524	0.627295	0.732467
	SHEAR	0.119353	0.734466	0.989392
	Average	0.09418	0.65831	0.84945

Furthermore, the IO, LS, and CP capacities of the models could also be estimated using IDA. According to Table 12 and Figs. 18-20, the models had almost the same IO limit, unlike the LS and CP limits. For the three-story SPSWs, the SHEAR model had higher LS performance than FLEX and INT (see Fig. 18), while FLEX and INT had almost the same LS performance. The CP performance was in the order of SHEAR>FLEX>INT. For the six-story SPSWs, the SHEAR model

had substantially larger CP and LS capacities than FLEX and INT (see Fig. 19), while the FLEX and INT models had almost the same LS and CP capacities. SHEAR and FLEX had the highest and lowest LS performance for the nine-story SPSWs, respectively, while the highest and lowest CP performance corresponded to SHEAR and INT, respectively (see Fig. 20).

According to Table 12, the models had almost the same accelerations for a given number of stories. Collapse capacity estimation and design validation are major contributions of IDA curves. FEMA P-695 defines the collapse margin ratio (CMR) as the ratio of the median 5%-damped spectral acceleration of collapse-level ground motions to the 5%-damped spectral acceleration of the MCE ground motions:

$$CMR = \frac{\hat{S}_{CT}}{S_{MT}} \tag{15}$$

The CMR is scaled and modified by the spectral shape factor (SSF), which is obtained from the period and ductility under FEMA P-695. Then, the ACMR is calculated as [28]:

$$ACMR = SSF * CMR \tag{16}$$

To validate the design model, it is required to calculate and compare $ACMR_{10\%}$ and $ACMR_{20}$ to $\overline{ACMR_i}$ and $ACMR_i$. To estimate $ACMR_{10\%}$ and $ACMR_{20}$, total system collapse uncertainty β_{TOT} should be calculated. Numerous uncertainty factors lead to variations in collapse capacity. Greater variability in collapse predictions requires larger margins to maintain an acceptable collapse probability at the MCE intensity. It is crucial to assess all major sources of uncertainty in collapse response and include their impacts in the collapse evaluation process. It is obtained from four other uncertainty parameters, including the record-to-record uncertainty β_{RTR}^2, designed requirements-related uncertainty β_{DR}^2, test data-related uncertainty β_{TD}^2, and modeling-rated uncertainty β_{MDL}^2. According to Purba and Bruneau and Ma et al., β_{RTR}^2, β_{DR}^2, β_{TD}^2, and β_{MDL}^2 were set to 0.4, 0.2, 0.35, and 0.2, respectively [28,42,43]:

$$\beta_{TOT} = \sqrt{\beta_{RTR}^2 + \beta_{DR}^2 + \beta_{TD}^2 + \beta_{MDL}^2} \tag{17}$$

Based on FEMA P-695, $ACMR_{10\%}$ and $ACMR_{20\%}$ were calculated to be 2.16 and 1.66, respectively. As shown in Table 13, all models met the limits and criteria, suggesting that the design was reliable.

Table 13. Design evaluation of different models.

N-ST	Model	$\hat{S}_{CT}$	S_{MT}	CMR	SSF	$ACMR_i$	$\overline{ACMR_i}$	$ACMR_i > ACMR_{20\%}$	$\overline{ACMR_i} > ACMR_{10\%}$
3-ST	FLEX	1.44	0.74	1.95	1.31	2.55	2.97	Pass	Pass
	INT	1.39	0.7	1.99	1.38	2.74		Pass	
	SHEAR	1.64	0.65	2.52	1.43	3.61		Pass	
6-ST	FLEX	1.37	0.56	2.45	1.3	3.18	3.68	Pass	Pass
	INT	1.38	0.52	2.65	1.37	3.64		Pass	
	SHEAR	1.61	0.54	2.98	1.42	4.23		Pass	
9-ST	FLEX	0.83	0.45	1.84	1.41	2.60	3.07	Pass	Pass
	INT	0.73	0.35	2.09	1.45	3.02		Pass	
	SHEAR	0.99	0.41	2.41	1.49	3.60		Pass	

Figures 21-23 plot the fragility curves. As mentioned, SHREAR outperformed FLEX and INT, which ensured a lower failure probability at all hazard levels. Furthermore, the average data of LS, CP, and IO limits are innovatively provided (Table 12). Based on the average data, all models

showed almost good IO performance, consistent with time-history analysis. According to Fig. 21, for the three-story SPSW, INT was a better model for the LS level, while FLEX was a better model for the CP level. This difference may be attributed to the higher energy absorption and ductility of FLEX. For the six-story SPSWs, the opposite is the case (see Fig. 22); FLEX was better at the LS level, and INT was better at the CP level. For the nine-story SPSWs, FLEX outperformed INT at both CP and LS levels (see Fig. 23). Time-history analysis did not provide solid judgment, whereas IDA effectively rated the SPSWs in terms of performance. The static analysis, time-history analysis, and IDA analysis outputs suggest that SHEAR outperformed INT and FLEX. To identify the optimal model between FLEX and INT, the expected performance level and design cost are to be incorporated. It can be concluded that SHEAR and FLEX would be optimal for low- and high-rise SPSWs, respectively, while INT and SHEAR are more optimal for mid-rise SPSWs (e.g., the six-story SPSWs). As FLEX and INT had almost the same performance, it is recommended that FLEX be employed since it is more affordable.

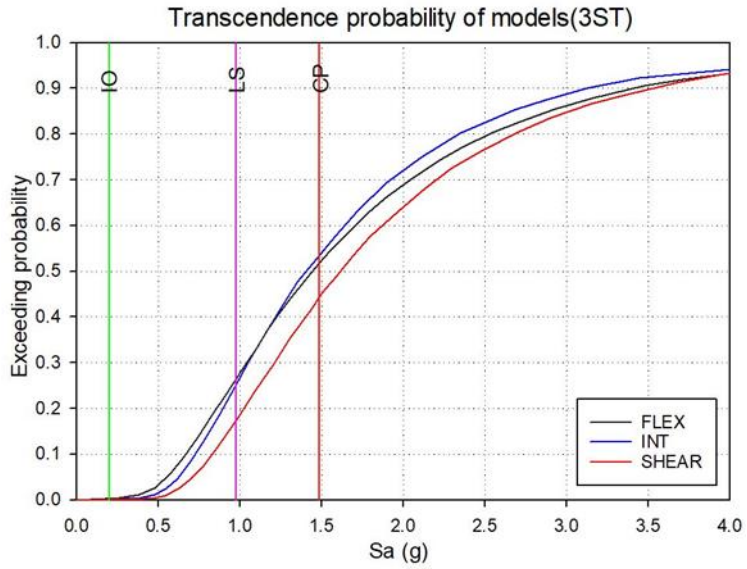

Fig. 21. Fragility curves of the 3-story SPSW under SHEAR, INT, and FLEX models.

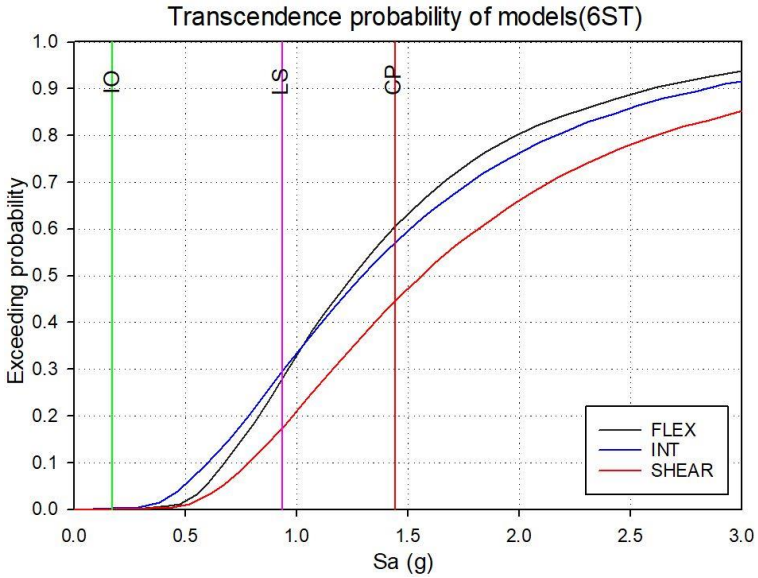

Fig. 22. Fragility curves of the 6-story SPSW under SHEAR, INT, and FLEX models.

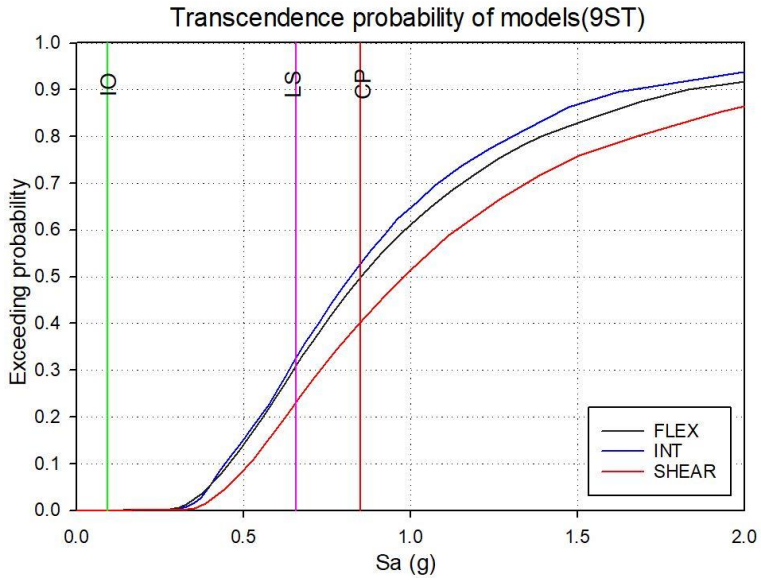

Fig. 23. Fragility curves of the 9-story SPSW under SHEAR, INT, and FLEX models.

The prioritization of coupling beam behaviors in SPSWs reflects their ability to meet diverse performance and economic objectives. Shear-dominated beams (SHEAR) were prioritized for high-rise SPSWs due to their superior stiffness and energy dissipation, critical for controlling inter-story drift and ensuring seismic safety in high-risk regions. Pushover analysis demonstrated that SHEAR beams effectively transfer lateral forces and distribute stresses uniformly across steel plates and boundary elements, with diagonal propagation of plastic hinges highlighting the efficient utilization of the tension field action. SHEAR models consistently exhibited higher initial stiffness and energy dissipation compared to FLEX and INT configurations, with the 9-story SHEAR model showing 99% greater stiffness than FLEX. Cyclic analyses further confirmed their enhanced plastic strength and energy absorption capabilities, while time-history analysis showed that SHEAR configurations maintained residual drifts within acceptable limits, ensuring better seismic safety and post-earthquake functionality. Incremental Dynamic Analysis (IDA) validated their robustness under extreme seismic conditions, with higher collapse margin ratios (CMR) compared to other configurations.

In contrast, flexural-shear beams (INT) offered a balanced solution for mid-rise buildings by combining moderate energy dissipation and drift control with reduced material demands. Flexural beams (FLEX), being less rigid and more cost-efficient, were suitable for low-rise structures in low-seismic regions or budget-constrained projects. While this study qualitatively addresses the tradeoff between performance and cost efficiency, a detailed structural cost analysis was beyond its scope. Nevertheless, the findings highlight that FLEX configurations minimize material and fabrication costs, making them practical for economical designs. Meanwhile, SHEAR configurations justify their higher costs by providing superior seismic resilience and robustness, ensuring safety and performance in critical applications for high-rise structures in high-seismic zones.

5. Conclusions

This study performed linear and nonlinear seismic analyses on coupled SPSWs with three, six, and nine stories in OpenSees and ABAQUS to evaluate their performance and identify the optimal

model at different performance levels (LS, CP, and IO) under FEMA P-695. The results can be summarized as:

(1) Pushover analysis suggested that the performance of the three models was in the order of SHEAR>INT>FLEX.
(2) Cyclic analysis demonstrated the seismic capacity of the models in the order of SHEAR>INT>FLEX. However, FLEX had a slightly smaller residual drift than SHEAR and INT (for three-, six-, and nine-story SPSWs).
(3) Time-history analysis indicated that SHEAR was the most optimal model in terms of the maximum drift and residual drift. However, the optimal model between FLEX and INT could not be identified.
(4) It was found that nonlinear static and nonlinear time-history analyses would not be effective for seismic evaluation, and more sophisticated approaches such as IDA are to be employed.
(5) IDA showed that SHEAR outperformed FLEX and INT, and the FLEX model would be economically more preferential than INT.

Funding

This research received no specific grant from any funding agency in the public, commercial, or not-for-profit sectors.

Conflicts of interest

The authors declare that they have no known competing financial interests or personal relationships that could have appeared to influence the work reported in this paper.

Authors contribution statement

Seyed Mohammad Ali Abbaspoor Haghighat: Conceptualization, Formal analysis, Validation, Software.

Ali Alibazi: Conceptualization; Data curation; Formal analysis; Investigation; Methodology,Roles/Writing – original draft.

Reza Moradifard: Formal analysis; Software; Visualization; Roles/Writing – original draft.

Lotfi Guizani: Project administration;; Supervision; Writing – review & editing.

Munzer Hassan: Project administration;; Supervision; Writing – review & editing.

References

[1] Thorburn LJ, Montgomery CJ, Kulak GL. Analysis of steel plate shear walls 1983.
[2] Qu B, Bruneau M. Design of Steel Plate Shear Walls Considering Boundary Frame Moment Resisting Action. J Struct Eng 2009;135:1511–21. https://doi.org/10.1061/(ASCE)ST.1943-541X.0000069.
[3] Wagner H. Flat sheet metal girders with very thin metal web. Part I: general theories and assumptions. 1931.

[4] Takahashi Y, Takemoto Y, Takeda T, Takagi M. Experimental study on thin steel shear walls and particular bracings under alternative horizontal load. Prelim. Report, IABSE, Symp. Resist. Ultim. Deform. Tsructures Acted by Well-defined Repeated Loads, Lisbon, Port., 1973, p. 185–91.

[5] Timler PA, Kulak GL. Experimental study of steel plate shear walls 1983.

[6] Tromposch EW, Kulak GL. Cyclic and static behaviour of thin panel steel plate shear walls 1987.

[7] Borello DJ, Fahnestock LA. Design and Testing of Coupled Steel Plate Shear Walls. Struct. Congr. 2011, Reston, VA: American Society of Civil Engineers; 2011, p. 736–47. https://doi.org/10.1061/41171(401)65.

[8] Borello DJ, Fahnestock LA. Behavior and mechanisms of steel plate shear walls with coupling. J Constr Steel Res 2012;74:8–16. https://doi.org/10.1016/j.jcsr.2011.12.009.

[9] Borello DJ, Fahnestock LA. Seismic Design and Analysis of Steel Plate Shear Walls with Coupling. J Struct Eng 2013;139:1263–73. https://doi.org/10.1061/(ASCE)ST.1943-541X.0000576.

[10] Gholhaki M, Ghadaksaz MB. Investigation of the link beam length of a coupled steel plate shear wall. Steel Compos Struct 2016;20:107–25.

[11] Pavir A, Shekastehband B. Hysteretic behavior of coupled steel plate shear walls. J Constr Steel Res 2017;133:19–35. https://doi.org/10.1016/j.jcsr.2017.01.019.

[12] Ma Z, Wu Y, Zhang J, Zhang M. Experimental Study on Seismic Behavior of Coupled Steel Plate and Reinforced Concrete Composite Wall. Buildings 2022;12:2036. https://doi.org/10.3390/buildings12112036.

[13] Farajian M, Khodakarami MI. The Influence of Inter-Connections Characteristics on the Lateral Performance of Braced-Frame Modular Steel Buildings. J Rehabil Civ Eng 2024;12:86–102. https://doi.org/10.22075/jrce.2023.31689.1894.

[14] Ma Y, Sun B, Berman JW, Taoum A, Yang Y. Cyclic behavior of coupled steel plate shear walls with different beam-to-column connections. J Constr Steel Res 2022;189:107084. https://doi.org/10.1016/j.jcsr.2021.107084.

[15] Mu Z, Yang Y. Experimental and numerical study on seismic behavior of obliquely stiffened steel plate shear walls with openings. Thin-Walled Struct 2020;146:106457. https://doi.org/10.1016/j.tws.2019.106457.

[16] Gorji Azandariani M, Gholhaki M, Kafi MA. Experimental and numerical investigation of low-yield-strength (LYS) steel plate shear walls under cyclic loading. Eng Struct 2020;203:109866. https://doi.org/10.1016/j.engstruct.2019.109866.

[17] Shayanfar M, Broujerdian V, Ghamari A. Analysis of Coupled Steel Plate Shear Walls with Outrigger System for Tall Buildings. Iran J Sci Technol Trans Civ Eng 2020;44:151–63. https://doi.org/10.1007/s40996-019-00246-2.

[18] Safari Gorji M, Cheng JJR. Plastic analysis and performance-based design of coupled steel plate shear walls. Eng Struct 2018;166:472–84. https://doi.org/10.1016/j.engstruct.2018.03.048.

[19] Abdollahzadeh G, Malekzadeh H. Response modification factor of coupled steel shear walls. Civ Eng Infrastructures J 2013;46:15–26.

[20] Wu X, Hao J, Tian W, Li S, Wang R. Cyclic tests and performance of weak-axis connected uncoupled and coupled steel plate shear wall with novel infill plate configuration. Thin-Walled Struct 2022;178:109331. https://doi.org/10.1016/j.tws.2022.109331.

[21] Hao J, Li S, Tian W, Wu X. Seismic performance of coupled steel plate shear wall with slits. J Constr Steel Res 2023;201:107674. https://doi.org/10.1016/j.jcsr.2022.107674.

[22] Kharmale SB, Ghosh S. Performance-based plastic design of steel plate shear walls. J Constr Steel Res 2013;90:85–97. https://doi.org/10.1016/j.jcsr.2013.07.029.

[23] Goel SC, Chao S-H. Performance-based plastic design: earthquake-resistant steel structures. (No Title) 2008.

[24] Moradifard R, Alibazi A, Shiravand MR, Gholami M. Improved performance-based plastic design method for post-tensioned connection systems. Eng Struct 2022;255:113931. https://doi.org/10.1016/j.engstruct.2022.113931.

[25] Liao WC, Goel SC. Performance-Based Seismic Design of RC SMF Using Target Drift and Yield Mechanism as Performance Criteria. Adv Struct Eng 2014;17:529–42. https://doi.org/10.1260/1369-4332.17.4.529.

[26] Chao S-H, Goel SC. Performance-based seismic design of EBF using target drift and yield mechanism as performance criteria. Ann Arbor 2005;1001:42125–8109.

[27] Fema. FEMA 355 State of the Art Report on Systems Performance of Steel Moment Frames Subject to Earthquake Ground Shaking. Rep No FEMA-355C 2000.

[28] FEMA P695 (2009). "Quantification of building seismic performance factors," Rep. FEMA P695, Federal Emergency Management Agency, Washington, D.C. n.d.

[29] McKenna F, Fenves GL, Scott MH. Open system for earthquake engineering simulation. Berkeley, CA: University of California; 2000 2014.

[30] Krawinkler H. ATC-24: Guidelines for cyclic seismic testing of components of steel structures. Redw City, Rep Prep Appl Technol Counc 1992.

[31] Choi I-R, Park H-G. Steel Plate Shear Walls with Various Infill Plate Designs. J Struct Eng 2009;135:785–96. https://doi.org/10.1061/(ASCE)0733-9445(2009)135:7(785).

[32] FEMA 355C (2000). "State of the Art Report on Systems Performance of Steel Moment Frames Subject to Earthquake Ground Shaking" Rep. FEMA P695, Federal Emergency Management Agency, Washington, D.C. n.d.

[33] Federal Emergency Managment Agency (FEMA), (2009). FEMA P695: Quantification of Building Seismic Performance Factors(Washigton, DC, USA). n.d.

[34] ASCE/SEI 7-10 . (2013). Minimum Design Loads for Buildings and Other Structures, American Society of Civil Engineers n.d.

[35] FEMA 356, 2000. NEHRP Guidelines for the seismic rehabilitation of buildings. Federal Emergency Management Agency. Washington DC n.d.

[36] Verma A, Sahoo DR. Estimation of lateral force contribution of boundary elements in steel plate shear wall systems. Earthq Eng Struct Dyn 2017;46:1081–98. https://doi.org/10.1002/eqe.2845.

[37] SEAOC. (1995). Vision 2000: Performance-Based Seismic Engineering of Buildings. Sacramento, CA: Structural Engineers Association of California n.d.

[38] Uang C. Establishing R (or Rw) and Cd Factors for Building Seismic Provisions. J Struct Eng 1991;117:19–28. https://doi.org/10.1061/(ASCE)0733-9445(1991)117:1(19).

[39] SAC. (2000). Seismic design criteria for steel moment-frame structures : FEMA 350, 351, 352 and 353 : Policy guide, FEMA 354 : State of the art reports, FEMA 355A, B, C, D, E and F. [Washington, D.C.] :FEMA : NEHRP n.d.

[40] Vamvatsikos D, Cornell CA. Incremental dynamic analysis. Earthq Eng Struct Dyn 2002;31:491–514. https://doi.org/10.1002/eqe.141.

[41] Bertero V V. Strength and deformation capacities of buildings under extreme environments. Struct Eng Struct Mech 1977;53:29–79.

[42] Purba R, Bruneau M. Seismic Performance of Steel Plate Shear Walls Considering Two Different Design Philosophies of Infill Plates. II: Assessment of Collapse Potential. J Struct Eng 2015;141. https://doi.org/10.1061/(ASCE)ST.1943-541X.0001097.

[43] Bhowmick AK, Driver RG, Grondin GY. Application of Indirect Capacity Design Principles for Seismic Design of Steel-Plate Shear Walls. J Struct Eng 2011;137:521–30. https://doi.org/10.1061/(ASCE)ST.1943-541X.0000303.